広島大学学位請求論文

A study on the dynamin-2-dependent regulatory mechanisms of microtubule dynamics

(ダイナミン-２依存的微小管動態制御機構の解明に関する研究)

２０２２年

広島大学大学院統合生命科学研究科

生命医科学プログラム

郭　潤昭

目次

主論文

A study on the dynamin-2-dependent regulatory mechanisms of microtubule dynamics

(ダイナミン-２依存的微小管動態制御機構の解明に関する研究)

CONTENTS

Abstract

Microtubule stability and dynamics regulations are essential for vital cellular processes, such as microtubule-dependent axonal transport. Dynamin is involved in many membrane fission events, such as clathrin-mediated endocytosis. The ubiquitously expressed dynamin-2 has been reported to regulate microtubule stability. However, the underlying molecular mechanisms remain unclear. This study aimed to investigate the roles of intrinsic properties of dynamin-2 on microtubule regulation by rescue experiments. A heterozygous *DNM2* mutation in HeLa cells was generated, and an increase in the level of stabilized microtubules in these heterozygous cells was observed. The expression of wild-type dynamin-2 in heterozygous cells reduced stabilized microtubules. Conversely, the expression of self-assembly-defective mutants of dynamin-2 in the heterozygous cells failed to decrease stabilized microtubules. This indicated that the self-assembling ability of dynamin-2 is necessary for regulating microtubule stability. Moreover, the heterozygous cells expressing the GTPase-defective dynamin-2 mutant, K44A, reduced microtubule stabilization, similar to the cells expressing wild-type dynamin-2, suggesting that GTPase activity of dynamin-2 is not essential for regulating microtubule stability. These results showed that the mechanism of microtubule regulation by dynamin-2 is diverse from that of endocytosis.

Keywords: Dynamin-2, endocytosis, GTPase activity, microtubule stability, self-assembly

Introduction

Microtubules are highly dynamic structural filaments that direct cellular morphology, migration, and cell division. Microtubules are commonly divided into two functional fractions: dynamic and stable microtubules (Avila, 1992). Dynamic microtubules demonstrate rapid exchange of tubulin subunits, leading to elongating and shrinking microtubules. In specialized cells, such as neurons, microtubules form stable bundles within axons and facilitate the transport of synaptic vesicles. Hyperdynamic microtubules have been observed in many neurodegenerative diseases, such as Alzheimer's disease and amyotrophic lateral sclerosis. In contrast, increased microtubule stability triggers the progression of neurodegeneration in hereditary spastic paraplegia (Dubey, Ratnakaran, & Koushika, 2015). Thus, the dysregulation of microtubule stability contributes to the progression of various diseases. Although microtubule-associated proteins, such as MAP2 and tau, have been reported to stabilize microtubules by inhibiting their depolymerization (Dehmelt & Halpain, 2005), the regulatory mechanisms of microtubule stability remain poorly understood.

Classical dynamin is conserved in many organisms, including *Caenorhabditis elegans*, *Drosophila melanogaster*, and mammals (Clark, Shurland, Meyerowitz, Bargmann, & van der Bliek, 1997). For example, dynamin in *C. elegans* and *D. melanogaster* is encoded by *dyn-1* and *shibire*, respectively (Clark et al., 1997). There are three classical dynamins in mammals, dynamin-1, dynamin-2, and dynamin-3, encoded by three genes viz. *DNM1*, *DNM2*, and *DNM3*, respectively. Dynamin-1 primarily functions in the brain and nerves; dynamin-2 is ubiquitously expressed; dynamin-3 is expressed in the testes, lungs, heart, and brain (Nakata et al., 1993; Sontag et al., 1994). Three dynamins are identical to each other, especially at the amino-terminus, and they share approximately

80% identity at the full-length protein level (T. A. Cook et al., 1994; T. Cook et al., 1996; Nakata et al., 1993).

Dynamin mutants contribute to various human diseases. For instance, many *DNM2* mutations have been identified from subtypes of Charcot–Marie–Tooth (CMT) neuropathy, CMT2M (Fabrizi et al., 2007), CMTDIB (Züchner et al., 2005), and type 1 of centronuclear myopathy (CNM) (Bitoun et al., 2005).

Dynamin consists of five domains, including GTPase, middle, pleckstrin homology (PH), GTPase effector (GE), and proline-rich (PR) domains. It was reported that *shibire* supports receptor-mediated endocytosis (Chen et al., 1991; van der Bliek & Meyerowrtz, 1991), suggesting functional roles of dynamins *in vivo*. The dominant negative mutant, K44A of mammalian dynamin abolished their internalization of transferrin due to impairment of clathrin-mediated endocytosis (Damke et al., 1994). In addition, dynamin also participates in other endocytic events, such as caveolin-dependent endocytosis (Henley et al., 1998; Oh et al., 1998) and fluid-phase endocytosis (Cao et al., 2007). During endocytosis process, dynamin can spontaneously self-assemble into rings or helices around the neck of the clathrin-coated pits (Hinshaw & Schmid, 1995; Takei, McPherson, Schmid, & Camilli, 1995), realized by the strong interaction between the middle and GE domains within and between dynamin dimers (Zhang & Hinshaw, 2001). GTP binding and hydrolysis are required to drive a conformational change in dynamin (Takei et al., 1995), resulting in vesicle detachment from the plasma membrane. GTPase activity can be triggered by dynamin self-assembly (Warnock, Hinshaw, & Schmid, 1996) or other activators, such as microtubules (Herskovits et al., 1993). Additionally, dynamin is associated with the cytoskeleton, including actin filaments (McNiven et al., 2000) and microtubules (Shpetner & Vallee, 1989). Purified dynamin from the bovine brain has

shown microtubule binding and bundling properties *in vitro* (Shpetner & Vallee, 1989). The co-localization of dynamin and microtubules is also observed in cells and *in vivo* (Thompson, Skop, Euteneuer, Meyer, & McNiven, 2002; Züchner et al., 2005). Furthermore, the ubiquitously expressed dynamin-2 in mammals regulates microtubules. Overexpression of a CMT disease-related dynamin-2 mutant, 551Δ3, increases the level of stabilized microtubules in cultured cells (Tanabe & Takei, 2009). Despite evidence for dynamin–microtubule interaction, the regulatory mechanism of microtubule stability by dynamin-2 is still unclear.

This study investigated the regulatory mechanisms of microtubule stability by dynamin-2 in HeLa cells using rescue experiments. First, I generated a heterozygous *DNM2* mutant cell line (*DNM2*$^{HLD>R/-}$ HeLa cells) with depleted endogenous dynamin-2 protein and increased stabilized microtubules. Then, I examined the effect of disease-related dynamin-2 mutants on microtubule stability by expressing GFP-dynamin-2 constructs in these heterozygous cells. Using the same method, I also investigated the necessity of each domain of dynamin-2 during microtubule regulation. Furthermore, the properties of dynamin-2, including GTPase activity and self-assembling ability, which are essential for clathrin-mediated endocytosis, were studied by expressing the function-defective mutants in *DNM2*$^{HLD>R/-}$ HeLa cells.

Materials and Methods

Materials and chemicals

Mouse monoclonal anti-acetylated tubulin antibody (#T6793, diluted 1:2000 for immunoblotting and 1:500 for immunofluorescence) and alkaline phosphatase-conjugated rabbit anti-goat IgG (#AP106A, diluted 1:5000 before use) were purchased from Merck (Darmstadt, Germany). Goat polyclonal anti-dynamin-2 antibody (#sc-6400, diluted 1:200 before use) was purchased from Santa Cruz Biotechnology, Inc. (CA, USA). Mouse monoclonal anti-actin antibody (#ab14128, diluted 1:2000 before use) was purchased from Abcam (Cambridge, UK). Mouse anti-α-tubulin antibody (clone DM1A, #CLT9002, diluted 1:2000 before use) was purchased from CEDARLANE (Ontario, Canada). Alexa Fluor 555 conjugated goat anti-mouse IgG (H+L) (#A-21424, diluted 1:400 before use) was purchased from Thermo Fisher Scientific (MA, USA). Alkaline phosphatase-conjugated anti-mouse IgG (#S372B, diluted 1:5000 before use) was purchased from Promega Corporation (WI, USA). Cy3-conjugated human transferrin (#009-160-050) was purchased from Jackson ImmunoResearch Laboratories (PA, USA).

Plasmid constructions

pEGFP-C1-*DNM2*-wild-type (WT) and pEGFP-C1-*DNM2*-K44A were previously generated (Hamao, Morita, & Hosoya, 2009). pEGFP-C1-*DNM2*-HLD>R, -ΔGTPase, -ΔMiddle, -ΔPH, -ΔGE, -ΔPR, -R361S, -K535A, -551Δ3, -555Δ3, -G537C, -K562E, -A618T, -S619L, or -I684K, was generated by PCR-based mutagenesis using pEGFP-C1-*DNM2*-WT as a template using KOD One PCR Master Mix (#KMM-101; TOYOBO CO., LTD., Osaka, Japan). pGedit-*DNM2*-target, used for genome editing, was generated as described previously (Nagasaki et al., 2018).

Cell culture and transfection

HeLa cells (RCB0007) were procured from RIKEN BRC through the National Bio-Resource Project of MEXT/AMED, Japan. Cells were cultured in Eagle's Minimum Essential Medium (#5900; Nissui Pharmaceuticals Co., LTD., Tokyo, Japan) supplemented with 10% (v/v) fetal bovine serum (#8048; Biological Industries, Beit-Haemek, Israel) at 37℃ in a 5% CO_2 humidified atmosphere. Plasmid transfection was performed using Lipofectamine LTX Reagent (#15338-100; Thermo Fisher Scientific) as per the manufacturer's protocol.

Genome editing

The heterozygous *DNM2* mutant HeLa cell line (*DNM2*$^{HLD>R/-}$ cell line) was generated using the CRISPR/Cas9 system (Ran et al., 2013). First, the pGedit-*DNM2*-target plasmid containing Cas9, sgRNA, and EGFP-Blasticidin S-resistance gene was transfected into HeLa cells. Blasticidin S-resistant cell colonies were then picked up individually to generate cell lines. Finally, genomic DNA sequencing was performed to determine the genotype. Briefly, Genomic DNA containing the edited region was amplified with primers (Forward: 5'- GCCTGAGAACCGGATGAG -3'; Reverse: 5'- GCACCTCCTGTCCTACGG -3') by PCR using KOD One PCR Master Mix (#KMM-101; TOYOBO). The amplified DNA was electrophoresed and purified using Wizard SV Gel and PCR Clean-Up System (#A9281; Promega). The purified DNA was sequenced with a primer (Forward: 5'- GCCTGAGAACCGGATGAG -3').

Immunoblotting

Immunoblotting was performed as reported previously (Hamao et al., 2009). Briefly, cells were lysed in RIPA buffer (50 mM Tris–HCl, 150 mM NaCl, 0.1% SDS, 0.5% sodium deoxycholate, 1% Triton X-100, pH8.0) with 1× protease inhibitor (Complete Protease Inhibitor Cocktail, #4693116001; Merck) and 1 mM phenylmethylsulfonyl fluoride and sonicated on ice using a Branson 450 Sonifier (Branson Ultrasonics, CT, USA). The cell lysates were treated with Laemmli buffer (1% SDS, 50 mM dithiothreitol, 7.5% glycerol, 40 mM Tris–HCl, and bromophenol blue, pH 6.8) and boiled for 5 min to denature the proteins. Proteins were separated by SDS polyacrylamide gel electrophoresis and then transferred to a PVDF membrane (#ISEQ00010; Merck). Membranes were probed with anti-actin, anti-dynamin-2, or anti-acetylated tubulin antibodies, followed by alkaline phosphatase-conjugated secondary antibodies. Finally, the blots were developed with 0.2 mg/mL Nitro Blue Tetrazolium Chloride (#24720-56; NACALAI TESQUE, INC., Tokyo, Japan) and 0.1 mg/mL 5-bromo-4-chloro-3-indolyl phosphate p-toluidine salt (#05643-24; NACALAI TESQUE, INC.) in the alkaline phosphatase buffer (100 mM Tris–HCl, 5 mM $MgCl_2$, 100 mM NaCl, pH 9.5). Fiji software (v.1.53c; NIH, MD, USA) was used to analyze the gray value of protein bands.

Indirect immunofluorescence

Indirect immunofluorescence was performed as described previously (Hamao et al., 2009; Kondo et al., 2012). Briefly, cells on a coverslip were fixed with 3.7% formaldehyde and permeabilized with 0.2% Triton X-100. The cells were then probed with anti-acetylated tubulin or anti-α-tubulin antibody, followed by Alexa Fluor 555-conjugated secondary antibodies. Finally, the cells were mounted with Vectashield

mounting medium (#H-1000; Vector Laboratories, Inc., CA, USA). containing 0.5 mg/ml 4’6’-diamidine-2’-phenylindole dihydrochloride (DAPI) (NACALAI TESQUE, INC.). For cold resistance analysis, the cells were incubated on ice for the indicated time and fixed with 3.7% formaldehyde for subsequent staining.

Microscopy

Images of rescue experiments were obtained using a confocal microscope (Olympus FV1000; Olympus, Tokyo, Japan) with UPLSAPO 40×/NA 0.90 objective (Olympus), using 473 nm and 559 nm laser lines. Images of cold resistance experiment were obtained using ZEISS LSM 900 (Carl Zeiss AG, Oberkochen, Germany) with Plan-Apochromat 63×/1.40 Oil M27 objective (Zeiss), using 488 nm and 561 nm laser lines. CellProfiler software (v.4.0.7; Broad Institute, MA, USA) and ImageJ software (v.1.53c, NIH) were used to measure the fluorescence intensity of acetylated tubulin and internalized transferrin. In brief, GFP channel was used to determine the outline of the individual cell, and the integrated density in acetylated tubulin channel of each cell was measured.

Statistical analysis

GraphPad Prism v.7.03 (GraphPad Software, Inc., CA, USA) was used to perform the statistical analysis. Statistical significance was assessed as described in the individual figure legends.

Results

Dynamin-2 is involved in regulating microtubule stability

To confirm that dynamin-2 regulates microtubule stability in HeLa cells, I attempted to generate a *DNM2* knock-out cell line using the CRISPR/Cas9 system. The target mutation sequence of *DNM2* was designed in exon 1 or 2, and 5 out of 12 single-cell clones could survive and proliferate. I determined the genotypes of the 5 clones, but none of them had homozygous mutations. Instead, 2 clones had no mutation, whereas the other three clones showed diverse heterozygous mutations. It suggested that dynamin-2 is too essential in multiple processes to be removed completely. Therefore, the one generated by targeting exon 1 (Fig. 1A) was used in the subsequent experiments. One allele of the *DNM2* gene in heterozygous mutant HeLa cells had a 190-base-pair deletion before the PAM sequence (Fig. 1B), suggesting that this allele could not produce the precise dynamin-2 protein. The other allele had a 6-base-pair deletion followed by a single base-pair substitution, resulting in a 2-amino-acid deletion and a 1-amino-acid change, which finally generated a mutation, HLD to R (HLD>R, Fig. 1B). Hence, the heterozygous *DNM2* mutant HeLa cells were termed as *DNM2*$^{\mathrm{HLD>R/-}}$ HeLa cells. Furthermore, the immunoblotting studies revealed that the expression of endogenous dynamin-2 was decreased by half in *DNM2*$^{\mathrm{HLD>R/-}}$ HeLa cells compared with that in control HeLa cells (Fig. 2A and B).

To assess microtubule stability, I quantified the level of acetylated α-tubulin, a marker of stabilized microtubules (Palazzo, Ackerman, & Gundersen, 2003). *DNM2*$^{\mathrm{HLD>R/-}}$ HeLa cells demonstrated high levels of stabilized microtubules compared with control HeLa cells by immunoblotting (Fig. 2A and B) and immunostaining (Fig. 2C and D). This result is consistent with that of previous work (Tanabe & Takei, 2009), and siRNA-mediated

dynamin-2 knockdown (Fig. 2E and F). The level of stabilized microtubules was examined in *DNM2*$^{HLD>R/-}$ HeLa cells expressing GFP-dynamin-2-WT or -HLD>R mutant (Fig. 3A). *DNM2*$^{HLD>R/-}$ HeLa cells expressing GFP-dynamin-2-WT decreased the levels of stabilized microtubules (Fig. 3B and C), confirming that dynamin-2 is involved in regulating microtubule stability. Similarly, *DNM2*$^{HLD>R/-}$ HeLa cells expressing GFP-dynamin-2-HLD>R exhibit a normal level of stabilized microtubule similar to the cells expressing GFP-dynamin-2-WT (Fig. 3B and C), suggesting that the increase in stabilized microtubules in *DNM2*$^{HLD>R/-}$ HeLa cells is not caused by the amino acid changes of dynamin-2 (HLD>R) from one of the *DNM2* alleles. To further examine the microtubule stability in *DNM2*$^{HLD>R/-}$ HeLa cells, I assessed the cold resistance of microtubules. The number of cells retaining more than one filamentous structure was quantified. After cold treatment for 30 min, the microtubules in 40% of the control cells were completely depolymerized. In contrast, approximately 80% of the *DNM2*$^{HLD>R/-}$ HeLa cells still have filamentous microtubules (Fig. 3D and E). It also indicated that microtubules are more stable in *DNM2*$^{HLD>R/-}$ HeLa cells. Consequently, these results demonstrated that dynamin-2 plays a vital role in regulating the transformation of stabilized microtubules to dynamic microtubules.

The Charcot–Marie–Tooth-related dynamin-2-551Δ3 mutant associates with microtubule stability.

Dynamin-2 is identified as the causative gene of CMT disease and CNM. A deletion mutant, 551Δ3, identified from a patient with CMT disease, co-localized with microtubules apparently, and overexpression of this mutant induced accumulation of stabilized microtubules in COS-7 cells (Tanabe & Takei, 2009). Therefore, I examined

whether dynamin-2-551Δ3 rescues microtubules in *DNM2*$^{HLD>R/-}$ HeLa cells. Expression of GFP-dynamin-2-551Δ3 in *DNM2*$^{HLD>R/-}$ HeLa cells did not reduce stabilized microtubules compared with dynamin-2-WT-expressing cells (Fig. 4A, B, and C). This result confirmed that 551Δ3 mutant leads to abnormal microtubule stabilization. Furthermore, I prepared dynamin-2-555Δ3, the longest splice variant of dynamin-2, with deletion of the identical residues as 551Δ3. *DNM2*$^{HLD>R/-}$ HeLa cells expressing 555Δ3 mutant had stabilized microtubules (Fig. 4A, D, and E), similar to the cells expressing 551Δ3 mutant (Fig. 4B and C), indicating an identical function in microtubule regulation between the different splice variants.

Additionally, I wondered whether the other disease mutants, including CMT mutants, G537C and K562E, and CNM mutants, A618T and S619L (Fig. 5A), display the regulatory effect on microtubules in *DNM2*$^{HLD>R/-}$ HeLa cells. As result of quantification, all CMT- and CNM-related mutants exhibited comparable levels of stabilized microtubules with dynamin-2-WT (Fig. 5B and C) in *DNM2*$^{HLD>R/-}$ HeLa cells. Both K562E and G537C mutants show impaired phosphoinositide-binding affinity (Chin et al., 2015; Kenniston & Lemmon, 2010) and defective transferrin uptake (Fig. 6A and B). However, the impairment of transferrin uptake was not observed in 551Δ3-expressing cells (Tanabe & Takei, 2009). Therefore, I concluded that the disorder in CMT patients with 551Δ3 mutation is linked to abnormal microtubule stability, distinct from other CMT-related mutants that disrupt endocytosis.

GTPase, middle, pleckstrin homology, and GTPase effector domains of dynamin-2 are required for regulating microtubule stability

To investigate the functional significance of the individual domains of dynamin-2 in

regulating microtubule stability, each dynamin-2 mutant lacking the individual GTPase, middle, PH, GE, and PR domains (Fig. 7A) was overexpressed in *DNM2*$^{HLD>R/-}$ HeLa cells. The *DNM2*$^{HLD>R/-}$ HeLa cells expressing GFP-dynamin-2-ΔGTPase, -ΔMiddle, -ΔPH, or -ΔGE remained at a high level of stabilized microtubules (Fig. 7B and C). Nevertheless, overexpression of GFP-dynamin-2-ΔPR reduced the level of stabilized microtubules in *DNM2*$^{HLD>R/-}$ HeLa cells (Fig. 7B and C). A previous study has suggested that the PR domain of dynamin is a significant interaction site for microtubules *in vitro* (Herskovits et al., 1993). Furthermore, dynamin-2 is localized along the mitotic spindle via the PR domain (Ishida, Nakamura, Tanabe, Li, & Takei, 2011). To examine whether the PR domain of dynamin-2 is also required to bind to interphase microtubule, I observed the co-localization of GFP-dynamin-2-WT and -ΔPR mutant with microtubules in HeLa cells. GFP-dynamin-2-WT appeared dotted structures along filaments after the removal of cytosolic proteins, while GFP-dynamin-2-ΔPR mutant showed dotted structures dispersed throughout the cell (Fig. 8A). In addition, I also observed reduced association between dynamin-2-ΔPR mutant and microtubules by performing Pearson correlation analysis (Fig. 8B), indicating that PR domain is involved in microtubule binding in cells, although it has no effect on microtubule regulation. Taken together, these findings suggested that the GTPase, middle, PH, and GE domains, but not the PR domain of dynamin-2 play vital roles in regulating microtubule stability.

Self-assembling ability of dynamin-2 participates in regulating microtubule stability

The middle and GE domains are located at the stalk structure of the dynamin-1 dimer (Zhang & Hinshaw, 2001). Dynamin-1 lacking GE domain expressed in COS-7 cells abolished self-assembly and reduced the sedimentation coefficient from 7.5S to 4.5S,

suggesting that the deletion of GE domain abolished self-assembly of dynamin-1 without aggregation (Okamoto, Tripet, Litowski, Hodges, & Vallee, 1999; Smirnova, Shurland, Newman-Smith, Pishvaee, & van der Bliek, 1999). Either middle or GE domain deletion dynamin-2 mutant exhibited a high level of stabilized microtubules (Fig. 7B and C). Therefore, I was curious about the necessity of self-assembling ability on microtubule regulation. Previous studies have reported that R361S in the middle domain (Ramachandran et al., 2007) or I690K in the GE domain (Song, Yarar, & Schmid, 2004) in dynamin-1 resulted in an unassembled protein. Accordingly, mutations were generated at the identical residues (R361S and I684K) in dynamin-2 (Fig. 9A), equivalent to dynamin-1-R361S and -I690K, respectively. Subsequently, the effects of these mutations on receptor-mediated endocytosis were assessed. The dominant-negative mutant, K44A, with impaired GTPase activity, was used as a positive control, as the inhibition of endocytosis has been observed in dynamin-2-K44A expressing cells (Altschuler et al., 1998). The results demonstrated that HeLa cells expressing dynamin-2-R361S and -I684K exhibit impaired Cy3-transferrin uptake compared with dynamin-2-WT-expressing cells (Fig. 9B and C), indicating that these dynamin-2 mutants induce endocytosis defects similar to those of dynamin-1. Then, I examined the level of stabilized microtubules in *DNM2*$^{HLD>R/-}$ HeLa cells expressing GFP-dynamin-2-R361S or -I684K, and none of them reduced the level of stabilized microtubules (Fig. 10A and B). These results demonstrated that the self-assembling ability of dynamin-2 is needed to regulate microtubule stability.

GTPase activity of dynamin-2 is unimportant for regulating microtubule stability

To examine the role of the GTPase activity of dynamin-2 on microtubule stability, the

GTPase-defective mutant, K44A (Damke et al., 1994), was overexpressed in *DNM2*$^{HLD>R/-}$ HeLa cells, and the levels of stabilized microtubules were assessed. The results revealed that stabilized microtubules in GFP-dynamin-2-K44A (Fig. 11A) overexpressing *DNM2*$^{HLD>R/-}$ HeLa cells were reduced to a normal level, as observed in *DNM2*$^{HLD>R/-}$ HeLa cells expressing GFP-dynamin-2-WT (Fig. 11B and C). Consistently, the CMT-related mutants K562E, which exhibited low stimulated-GTPase activity due to abolished phosphoinositide affinity (Kenniston & Lemmon, 2010), also demonstrated a reduction in the level of stabilized microtubules in *DNM2*$^{HLD>R/-}$ HeLa cells (Fig. 5B and C). These results suggested that the GTPase activity is not essential for microtubule regulation. Due to the necessity of GTPase activity for receptor-mediated endocytosis, I concluded that the mechanism of microtubule regulation by dynamin-2 is different from that of endocytosis regulation.

Discussion

The summary of this study

In this study, I have demonstrated that self-assembling ability, but not the GTPase activity, of dynamin-2 plays a significant role in regulating microtubule stability. The regulatory mechanism of microtubule stability by dynamin-2 differs from that of endocytosis since GTPase activity of dynamin-2 is required for the endocytosis, but not regulating microtubule stability (Fig. 12).

The tools and methods used in this study

In this study, I generated dynamin-2-depleted HeLa cells. HeLa cells were used because microtubule dynamics can be observed easily, and they proliferate faster than other cell types. I tried to generate dynamin-2 knock-out cells by CRISPR/Cas9 system, which is widely used for realizing genome editing. However, I failed to knock out dynamin-2 entirely. I consider that dynamin-2 is too essential in multiple processes, and complete depletion of dynamin-2 may induce cell death. Indeed, I found poor attachment of heterozygous mutant cells and observed slower growth of these cells than the parent HeLa cells. I thought it is due to the impairment of dynamin-2 function on focal adhesion and cytokinesis (Ezratty, Partridge, & Gundersen, 2005; Thompson et al., 2002). Endogenous dynamin-2 is decreased by half in the heterozygous mutant cells, and stabilized microtubules are increased significantly (Fig. 2A, B, C, and D). These results are consistent with that observed in siRNA-mediated dynamin-2 knockdown cells (Fig. 2E and F). Thus, the heterozygous mutant cell line is utilized as a useful tool for subsequent studies.

Tubulin acetylation was generally used as a marker of stable microtubules. However, recent studies support the sentiment that α-tubulin acetyl-transferase αTAT1 mediated acetylation can affect the structure and mechanical properties of microtubules (Eshun-Wilson et al., 2019). Although no evidence shows that dynamins interact with αTAT1 (Maruta, Greer, & Rosenbaum, 1986), to exclude the possibility that dynamin-2 regulates microtubules by interfering with tubulin acetylation, I also assessed microtubule stability using another method. I performed cold resistance analysis (Fig. 3D and E) and quantified the number of the cells with cold-resistant microtubules. Compared with control HeLa cells, more heterozygous cells have cold-resistant microtubules, supporting that dynamin-2 depletion results in more stabilized microtubules.

The role of dynamin-2 domains and biochemical properties in regulating microtubule stability

I summarized the roles of dynamin-2 domains and biochemical properties in regulating microtubule stability in Table 1. I have shown that overexpression of dynamin-2-551Δ3 or -555Δ3 mutant leads to abnormal microtubule stabilization in HeLa cells (Fig. 4), consistent with the previous result in COS-7 cells (Tanabe & Takei, 2009). On the other hand, low-level expression of the same mutant did not induce microtubule stabilization in embryonic fibroblasts from dynamin-2 conditional null mouse (Liu, Lukiyanchuk, & Schmid, 2011). The conflict between these reports may be caused by different cell types and expression levels of dynamin-2 mutant.

I have also shown that the PR domain of dynamin-2 is dispensable for regulating microtubule stability (Fig. 7B and C). Previously, it has been reported that a mammalian dynamin-like protein, DLP1, binds to single microtubules in cultured cells (Yoon, Pitts,

Dahan, & McNiven, 1998). Furthermore, another dynamin-related protein in plants, phragmoplastin, is associated with microtubules in various cell cycle phases (Hong, Geisler-Lee, Zhang, & Verma, 2003). Since both DLP1 and phragmoplastin lack the C-terminal PR domain, I wondered whether the PR domain of dynamin-2 is not involved in microtubules binding in cells. The co-localization analysis shows that dynamin-2-ΔPR mutant does not co-localize with microtubules in HeLa cells (Fig. 8A and B), consistent with an *in vitro* study that dynamin-1 binds to microtubules via the PR domain at the C-terminus (Herskovits et al., 1993). Conclusively, these results suggest that the PR domain is involved in microtubule binding and dynamin-2 regulates microtubule stability indirectly in cells, perhaps via interacting with additional factors.

Overexpression of the self-assembly-defective mutants, dynamin-2-R361S or -I684K, does not rescue microtubules in *DNM2*$^{HLD>R/-}$ HeLa cells (Fig. 10A and B). Sedimentation equilibrium analytical ultracentrifugation studies have shown that dynamin-1-R361S exists predominantly as a dimer, in contrast to the dynamin-1-WT tetramer (Ramachandran et al., 2007). It has been reported that dynamin-1-I690K mutant can form a tetramer, but not higher-order structures, such as a ring and a spiral (Song et al., 2004). Impaired endocytosis in dynamin-2-R361S- or -I684K-expressing cells (Fig. 9B and C) reveals that self-assembling ability is also abolished in mutated dynamin-2. Therefore, these results suggest the self-assembly-dependent regulation of microtubule stability by dynamin-2. Oligomeric dynamin has also been reported to crosslink F-actin filaments into regular bundles (Gu et al., 2010), indicating that oligomeric dynamin-2 may also be involved in crosslinking microtubules. It can be conjectured that oligomerized dynamin-2 is required to wrap around the microtubules, which inhibits the interaction between microtubule lattice and other stabilizing factors. Accordingly, the role

of self-assembled dynamin-2 in microtubule stability should be studied in more detail.

On the other hand, PH domain-mediated binding of dynamin to the phosphoinositide occurs coincident with, or following, its self-assembly (Klein, Lee, Frank, Marks, & Lemmon, 1998). Hence, the phosphoinositide-binding ability of dynamin-2 is a considerable property during microtubule regulation. In fact, I showed that dynamin-2-K535A (Fig. 13A), which essentially abolishes dynamin's phosphoinositide binding (Vallis, Wigge, Marks, Evans, & McMahon, 1999), did not decrease stabilized microtubule in *DNM2*$^{HLD>R/-}$ HeLa cells (Fig. 13B and C). However, an opposite effect was observed in another phosphoinositide-binding-defective mutant, K562E (Fig. 5B and C). Supportively, dynamin-1-K561M (equivalent to residue K562 in dynamin-2), but not K535M, binds to and is activated by microtubules (Achiriloaie, Barylko, & Albanesi, 1999), suggesting that the residue K535 is more critical for microtubule-binding than K561. Therefore, whether the phosphoinositide-binding ability is a crucial property for dynamin-2 on microtubule regulation remains a mystery, although K535 of dynamin-2 is required for microtubule stability.

The GTP binding and hydrolysis abilities of dynamin are commonly related to its functions in various cellular processes. For instance, during endocytosis, the force derived from GTP hydrolysis is used to change the conformation of dynamin oligomers, which form around the neck of budding vesicles (Takei et al., 1995). However, a decrease in the stabilized microtubules in dynamin-2-K44A-expressing *DNM2*$^{HLD>R/-}$ cells (Fig. 11B and C) demonstrates that the GTPase activity of dynamin-2 is not essential for regulating microtubule stability. In other words, the conformational change of dynamin-2 oligomers via GTP hydrolysis is not imperative for regulating microtubule stabilization. Interestingly, the complete deletion of the GTPase domain, containing the GTP binding

and hydrolysis site, K44, does not reduce the stabilized microtubules (Fig. 7B and C). Therefore, these findings indicate that the GTPase domain may have other functions, except for GTP binding and hydrolysis.

A hypothesis of the regulatory mechanism of dynamin-2-dependent microtubules

I hypothesize that dynamin-2 regulates microtubules by interacting factors. Candidate screening using *Drosophila* showed that *patronin* genetically interacts with dynamin homolog in *Drosophila, shibire*. Patronin is a microtubule minus-end binding protein, which was reported to protect microtubule minus end from depolymerization in *Drosophila* S2 cells (Goodwin & Vale, 2010). Introducing mutation in this protein rescued the lethal phenomenon in the flies that carry a disease-related mutation of dynamin-2 (data not shown), suggesting a genetical interaction between dynamin and Patronin. The Patronin homolog in human is CAMSAP family, which consists of three members, CAMSAP1, CAMSAP2, and CAMSAP3 (Baines et al., 2009). It has been reported that CAMSAP2/3 can slow down but do not block minus-end polymerization and inhibit minus-end disassembly (Akhmanova & Steinmetz, 2019). Furthermore, CAMSAP2 was also reported as a microtubule nucleation center in vitro (Imasaki et al., 2022). Therefore, dynamin-2 may suppress the stabilization or nucleation ability of CAMSAPs in cells. Depletion of dynamin-2 or expression of dynamin-2 mutants abolishes the suppression of stabilization or nucleation ability of CAMSAPs, resulting in more stabilized microtubules without growth and shrinkage, or just increasing the number of microtubules. More evidence is needed in the future to support this hypothesis.

Distinct functions of dynamin-1 and dynamin-2 on microtubule regulation

Mammalian dynamin has three members that function on different tissues. Three dynamins share approximately 80% identity at the full-length protein level, but they exhibit only 53% identity at C-terminus (Urrutia, Henley, Cook, & McNiven, 1997). In this study, depletion of dynamin-2 in HeLa cells induced abnormal stabilized microtubules, revealing that dynamin-2 is required for maintaining dynamic microtubules. In contrast to the effect of dynamin-2 on microtubules, depletion of dynamin-1 reduced the number of microtubule bundles in differentiated mouse podocyte (La et al., 2020), suggesting that dynamin-1 can stabilize microtubules. The low identity of the two PR domains of dynamin-1 and dynamin-2 may result in the opposite effect on microtubules, which is needed to be further studied by determining whether the two PR domains have distinct functions.

Acknowledgements

I’m very appreciative of my supervisor, Assoc. Prof. Kozue Hamao, who always inspires and supports me during my PhD study. She also encouraged me when I lost self-confidence. I want to thank Prof. Takahiro Chihara and Assoc. Prof. Misako Okumura for their insightful comments and advice. I’d like to thank Dr. Akira Nagasaki, Mr Ryuji Fujito and Ms. Mikiko Nakagushi for their contribution to this research. I also want to thank all members of my laboratory. Although I’m an international student, they make me feel like I'm not alone, and they often advise me when I am confused. I like everyone in cell biological laboratory. Finally, I would like to especially thank my boyfriend, Mr. Zhe Wang, for being with me in the past five years and understanding me.

References

Achiriloaie, M., Barylko, B., & Albanesi, J. P. (1999). Essential Role of the Dynamin Pleckstrin Homology Domain in Receptor-Mediated Endocytosis. *Molecular and Cellular Biology*, *19*(2), 1410. https://doi.org/10.1128/MCB.19.2.1410

Akhmanova, A., & Steinmetz, M. O. (2019). Microtubule minus-end regulation at a glance. *Journal of Cell Science*, *132*(11). https://doi.org/10.1242/JCS.227850/57303

Altschuler, Y., Barbas, S. M., Terlecky, L. J., Tang, K., Hardy, S., Mostov, K. E., & Schmid, S. L. (1998). Redundant and distinct functions for dynamin-1 and dynamin-2 isoforms. *The Journal of Cell Biology*, *143*(7), 1871–1881. https://doi.org/10.1083/jcb.143.7.1871

Avila, J. (1992). Microtubule functions. *Life Sciences*, *50*(5), 327–334. https://doi.org/10.1016/0024-3205(92)90433-P

Baines, A. J., Bignone, P. A., King, M. D. A., Maggs, A. M., Bennett, P. M., Pinder, J. C., & Phillips, G. W. (2009). The CKK Domain (DUF1781) Binds Microtubules and Defines the CAMSAP/ssp4 Family of Animal Proteins. *Molecular Biology and Evolution*, *26*(9), 2005–2014. https://doi.org/10.1093/MOLBEV/MSP115

Bitoun, M., Maugenre, S., Jeannet, P. Y., Lacène, E., Ferrer, X., Laforêt, P., … Guicheney, P. (2005). Mutations in dynamin 2 cause dominant centronuclear myopathy. *Nature Genetics*, *37*(11), 1207–1209. https://doi.org/10.1038/ng1657

Cao, H., Chen, J., Awoniyi, M., Henley, J. R., & McNiven, M. A. (2007). Dynamin 2 mediates fluid-phase micropinocytosis in epithelial cells. *Journal of Cell Science*, *120*(23), 4167–4177. https://doi.org/10.1242/JCS.010686

Chen, M. S., Obar, R. A., Schroeder, C. C., Austin, T. W., Poodry, C. A., Wadsworth, S. C., & Vallee, R. B. (1991). Multiple forms of dynamin are encoded by shibire, a Drosophila gene involved in endocytosis. *Nature 1991 351:6327*, *351*(6327), 583–586. https://doi.org/10.1038/351583a0

Chin, Y. H., Lee, A., Kan, H. W., Laiman, J., Chuang, M. C., Hsieh, S. T., & Liu, Y. W. (2015). Dynamin-2 mutations associated with centronuclear myopathy are hypermorphic and lead to T-tubule fragmentation. *Human Molecular Genetics*, *24*(19), 5542–5554. https://doi.org/10.1093/hmg/ddv285

Clark, S. G., Shurland, D. L., Meyerowitz, E. M., Bargmann, C. I., & van der Bliek, A. M. (1997). A dynamin GTPase mutation causes a rapid and reversible temperature-inducible locomotion defect in C. elegans. *Proceedings of the National Academy of Sciences of the United States of America*, *94*(19), 10438–10443. https://doi.org/10.1073/pnas.94.19.10438

Cook, T. A., Urrutia, R., & McNiven, M. A. (1994). Identification of dynamin 2, an isoform ubiquitously expressed in rat tissues. *Proceedings of the National Academy of Sciences of the United States of America*, *91*(2), 644–648. https://doi.org/10.1073/PNAS.91.2.644

Cook, T., Mesa, K., & Urrutia, R. (1996). Three Dynamin-Encoding Genes Are Differentially Expressed in Developing Rat Brain. *Journal of Neurochemistry*, *67*(3), 927–931. https://doi.org/10.1046/j.1471-4159.1996.67030927.x

Damke, H., Baba, T., Warnock, D. E., & Schmid, S. L. (1994). Induction of mutant dynamin specifically blocks endocytic coated vesicle formation. *The Journal of Cell Biology*, *127*(4), 915–934. https://doi.org/10.1083/jcb.127.4.915

Dehmelt, L., & Halpain, S. (2005). The MAP2/Tau family of microtubule-associated proteins. *Genome Biology*, Vol. 6, p. 204. BioMed Central. https://doi.org/10.1186/gb-2004-6-1-204

Dubey, J., Ratnakaran, N., & Koushika, S. P. (2015). Neurodegeneration and microtubule

dynamics: death by a thousand cuts. *Frontiers in Cellular Neuroscience*, *9*(September), 343. https://doi.org/10.3389/fncel.2015.00343

Eshun-Wilson, L., Zhang, R., Portran, D., Nachury, M. v., Toso, D. B., Löhr, T., … Nogales, E. (2019). Effects of α-tubulin acetylation on microtubule structure and stability. *Proceedings of the National Academy of Sciences of the United States of America*, *116*(21), 10366–10371. https://doi.org/10.1073/PNAS.1900441116/SUPPL_FILE/PNAS.1900441116.SAPP.PDF

Ezratty, E. J., Partridge, M. A., & Gundersen, G. G. (2005). Microtubule-induced focal adhesion disassembly is mediated by dynamin and focal adhesion kinase. *Nature Cell Biology*, *7*(6), 581–590. https://doi.org/10.1038/ncb1262

Fabrizi, G. M., Ferrarini, M., Cavallaro, T., Cabrini, I., Cerini, R., Bertolasi, L., & Rizzuto, N. (2007). Two novel mutations in dynamin-2 cause axonal Charcot-Marie-Tooth disease. *Neurology*, *69*(3), 291–295. https://doi.org/10.1212/01.wnl.0000265820.51075.61

Goodwin, S. S., & Vale, R. D. (2010). Patronin Regulates the Microtubule Network by Protecting Microtubule Minus Ends. *Cell*, *143*(2), 263–274. https://doi.org/10.1016/J.CELL.2010.09.022/ATTACHMENT/2927A7A9-7B61-4A14-99C3-38E4F9EF25C6/MMC7.MP4

Gu, C., Yaddanapudi, S., Weins, A., Osborn, T., Reiser, J., Pollak, M., … Sever, S. (2010). Direct dynamin–actin interactions regulate the actin cytoskeleton. *The EMBO Journal*, *29*(21), 3593–3606. https://doi.org/10.1038/emboj.2010.249

Hamao, K., Morita, M., & Hosoya, H. (2009). New function of the proline rich domain in dynamin-2 to negatively regulate its interaction with microtubules in mammalian cells. *Experimental Cell Research*, *315*(7), 1336–1345. https://doi.org/10.1016/J.YEXCR.2009.01.025

Henley, J. R., Krueger, E. W. A., Oswald, B. J., & McNiven, M. A. (1998). Dynamin-mediated Internalization of Caveolae. *Journal of Cell Biology*, *141*(1), 85–99. https://doi.org/10.1083/JCB.141.1.85

Herskovits, J. S., Shpetner, H. S., Burgess, C. C., & Vallee, R. B. (1993). Microtubules and Src homology 3 domains stimulate the dynamin GTPase via its C-terminal domain. *Proceedings of the National Academy of Sciences of the United States of America*, *90*(24), 11468–11472. https://doi.org/10.1073/pnas.90.24.11468

Hinshaw, J. E., & Schmid, S. L. (1995). Dynamin self-assembles into rings suggesting a mechanism for coated vesicle budding. *Nature*, *374*(6518), 190–192. https://doi.org/10.1038/374190a0

Hong, Z., Geisler-Lee, C. J., Zhang, Z., & Verma, D. P. S. (2003). Phragmoplastin dynamics: multiple forms, microtubule association and their roles in cell plate formation in plants. *Plant Molecular Biology*, *53*(3), 297–312. https://doi.org/10.1023/B:PLAN.0000006936.50532.3a

Imasaki, T., Kikkawa, S., Niwa, S., Saijo-Hamano, Y., Shigematsu, H., Aoyama, K., … Nitta, R. (2022). CAMSAP2 organizes a γ-tubulin-independent microtubule nucleation centre through phase separation. *ELife*, *11*. https://doi.org/10.7554/ELIFE.77365

Ishida, N., Nakamura, Y., Tanabe, K., Li, S. A., & Takei, K. (2011). Dynamin 2 associates with microtubules at mitosis and regulates cell cycle progression. *Cell Structure and Function*, *36*(2), 145–154. https://doi.org/10.1247/csf.10016

Kenniston, J. A., & Lemmon, M. A. (2010). Dynamin GTPase regulation is altered by PH domain mutations found in centronuclear myopathy patients. *The EMBO Journal*, *29*(18), 3054–3067. https://doi.org/10.1038/emboj.2010.187

Klein, D. E., Lee, A., Frank, D. W., Marks, M. S., & Lemmon, M. A. (1998). The Pleckstrin Homology Domains of Dynamin Isoforms Require Oligomerization for High Affinity Phosphoinositide Binding *. *Journal of Biological Chemistry*, *273*(42), 27725–27733. https://doi.org/10.1074/JBC.273.42.27725

Kondo, T., Isoda, R., Uchimura, T., Sugiyama, M., Hamao, K., & Hosoya, H. (2012). Diphosphorylated but not monophosphorylated myosin II regulatory light chain localizes to the midzone without its heavy chain during cytokinesis. *Biochemical and Biophysical Research Communications*, *417*(2), 686–691. https://doi.org/10.1016/j.bbrc.2011.11.151

La, T. M., Tachibana, H., Li, S. A., Abe, T., Seiriki, S., Nagaoka, H., … Yamada, H. (2020). Dynamin 1 is important for microtubule organization and stabilization in glomerular podocytes. *The FASEB Journal*, *34*(12), 16449–16463. https://doi.org/10.1096/FJ.202001240RR

Liu, Y. W., Lukiyanchuk, V., & Schmid, S. L. (2011). Common Membrane Trafficking Defects of Disease-Associated Dynamin 2 Mutations. *Traffic*, *12*(11), 1620–1633. https://doi.org/10.1111/J.1600-0854.2011.01250.X

Maruta, H., Greer, K., & Rosenbaum, J. L. (1986). The acetylation of alpha-tubulin and its relationship to the assembly and disassembly of microtubules. *Journal of Cell Biology*, *103*(2), 571–579. https://doi.org/10.1083/JCB.103.2.571

McNiven, M. A., Kim, L., Krueger, E. W., Orth, J. D., Cao, H., & Wong, T. W. (2000). Regulated interactions between dynamin and the actin-binding protein cortactin modulate cell shape. *Journal of Cell Biology*, *151*(1), 187–198. https://doi.org/10.1083/jcb.151.1.187

Nagasaki, A., Kato, Y., Meguro, K., Yamagishi, A., Nakamura, C., & Uyeda, T. Q. P. (2018). A genome editing vector that enables easy selection and identification of knockout cells. *Plasmid*, *98*(September), 37–44. https://doi.org/10.1016/j.plasmid.2018.08.005

Nakata, T., Takemura, R., & Hirokawa, N. (1993). A novel member of the dynamin family of GTP-binding proteins is expressed specifically in the testis. *Journal of Cell Science*, *105*(1), 1–5. https://doi.org/10.1242/jcs.105.1.1

Oh, P., McIntosh, D. P., & Schnitzer, J. E. (1998). Dynamin at the Neck of Caveolae Mediates Their Budding to Form Transport Vesicles by GTP-driven Fission from the Plasma Membrane of Endothelium. *Journal of Cell Biology*, *141*(1), 101–114. https://doi.org/10.1083/JCB.141.1.101

Okamoto, P. M., Tripet, B., Litowski, J., Hodges, R. S., & Vallee, R. B. (1999). Multiple distinct coiled-coils are involved in dynamin self-assembly. *Journal of Biological Chemistry*, *274*(15), 10277–10286. https://doi.org/10.1074/jbc.274.15.10277

Palazzo, A., Ackerman, B., & Gundersen, G. G. (2003). Cell biology: Tubulin acetylation and cell motility. *Nature*, *421*(6920), 230. https://doi.org/10.1038/421230a

Ramachandran, R., Surka, M., Chappie, J. S., Fowler, D. M., Foss, T. R., Song, B. D., & Schmid, S. L. (2007). The dynamin middle domain is critical for tetramerization and higher-order self-assembly. *The EMBO Journal*, *26*(2), 559–566. https://doi.org/10.1038/sj.emboj.7601491

Ran, F. A., Hsu, P. D., Wright, J., Agarwala, V., Scott, D. A., & Zhang, F. (2013). Genome engineering using the CRISPR-Cas9 system. *Nature Protocols*, *8*(11), 2281–2308. https://doi.org/10.1038/nprot.2013.143

Shpetner, H. S., & Vallee, R. B. (1989). Identification of dynamin, a novel mechanochemical enzyme that mediates interactions between microtubules. *Cell*, *59*(3), 421–432. https://doi.org/10.1016/0092-8674(89)90027-5

Smirnova, E., Shurland, D. L., Newman-Smith, E. D., Pishvaee, B., & van der Bliek, A. M.

(1999). A model for dynamin self-assembly based on binding between three different protein domains. *Journal of Biological Chemistry*, *274*(21), 14942–14947. https://doi.org/10.1074/jbc.274.21.14942

Song, B. D., Yarar, D., & Schmid, S. L. (2004). An assembly-incompetent mutant establishes a requirement for dynamin self-assembly in clathrin-mediated endocytosis in vivo. *Molecular Biology of the Cell*, *15*(5), 2243–2252. https://doi.org/10.1091/mbc.e04-01-0015

Sontag, J. M., Fykse, E. M., Ushkaryov, Y., Liu, J. P., Robinson, P. J., & Südhof, T. C. (1994). Differential expression and regulation of multiple dynamins. In *Journal of Biological Chemistry* (Vol. 269). United States: J Biol Chem. https://doi.org/10.1016/s0021-9258(17)41812-6

Takei, K., McPherson, P. S., Schmid, S. L., & Camilli, P. de. (1995). Tubular membrane invaginations coated by dynamin rings are induced by GTP-γS in nerve terminals. *Nature*, *374*(6518), 186–190. https://doi.org/10.1038/374186a0

Tanabe, K., & Takei, K. (2009). Dynamic instability of microtubules requires dynamin 2 and is impaired in a Charcot-Marie-Tooth mutant. *Journal of Cell Biology*, *185*(6), 939–948. https://doi.org/10.1083/jcb.200803153

Thompson, H. M., Skop, A. R., Euteneuer, U., Meyer, B. J., & McNiven, M. A. (2002). The large GTPase dynamin associates with the spindle midzone and is required for cytokinesis. *Current Biology*, *12*(24), 2111–2117. https://doi.org/10.1016/S0960-9822(02)01390-8

Urrutia, R., Henley, J. R., Cook, T., & McNiven, M. A. (1997). The dynamins: Redundant or distinct functions for an expanding family of related GTPases? *Proceedings of the National Academy of Sciences of the United States of America*, *94*(2), 377. https://doi.org/10.1073/PNAS.94.2.377

Vallis, Y., Wigge, P., Marks, B., Evans, P. R., & McMahon, H. T. (1999). Importance of the pleckstrin homology domain of dynamin in clathrin-mediated endocytosis. *Current Biology*, *9*(5), 257–260. https://doi.org/10.1016/S0960-9822(99)80114-6

van der Bliek, A. M., & Meyerowrtz, E. M. (1991). Dynamin-like protein encoded by the Drosophila shibire gene associated with vesicular traffic. *Nature*, *351*(6325), 411–414. https://doi.org/10.1038/351411a0

Warnock, D. E., Hinshaw, J. E., & Schmid, S. L. (1996). Dynamin self-assembly stimulates its GTPase activity. *Journal of Biological Chemistry*, *271*(37), 22310–22314. https://doi.org/10.1074/jbc.271.37.22310

Yoon, Y., Pitts, K. R., Dahan, S., & McNiven, M. A. (1998). A novel dynamin-like protein associates with cytoplasmic vesicles and tubules of the endoplasmic reticulum in mammalian cells. *Journal of Cell Biology*, *140*(4), 779–793. https://doi.org/10.1083/jcb.140.4.779

Zhang, P., & Hinshaw, J. E. (2001). Three-dimensional reconstruction of dynamin in the constricted state. *Nature Cell Biology*, *3*(10), 922–926. https://doi.org/10.1038/ncb1001-922

Züchner, S., Noureddine, M., Kennerson, M., Verhoeven, K., Claeys, K., de Jonghe, P., … Vance, J. M. (2005). Mutations in the pleckstrin homology domain of dynamin 2 cause dominant intermediate Charcot-Marie-Tooth disease. *Nature Genetics*, *37*(3), 289–294. https://doi.org/10.1038/ng1514

Figures

Figure 1

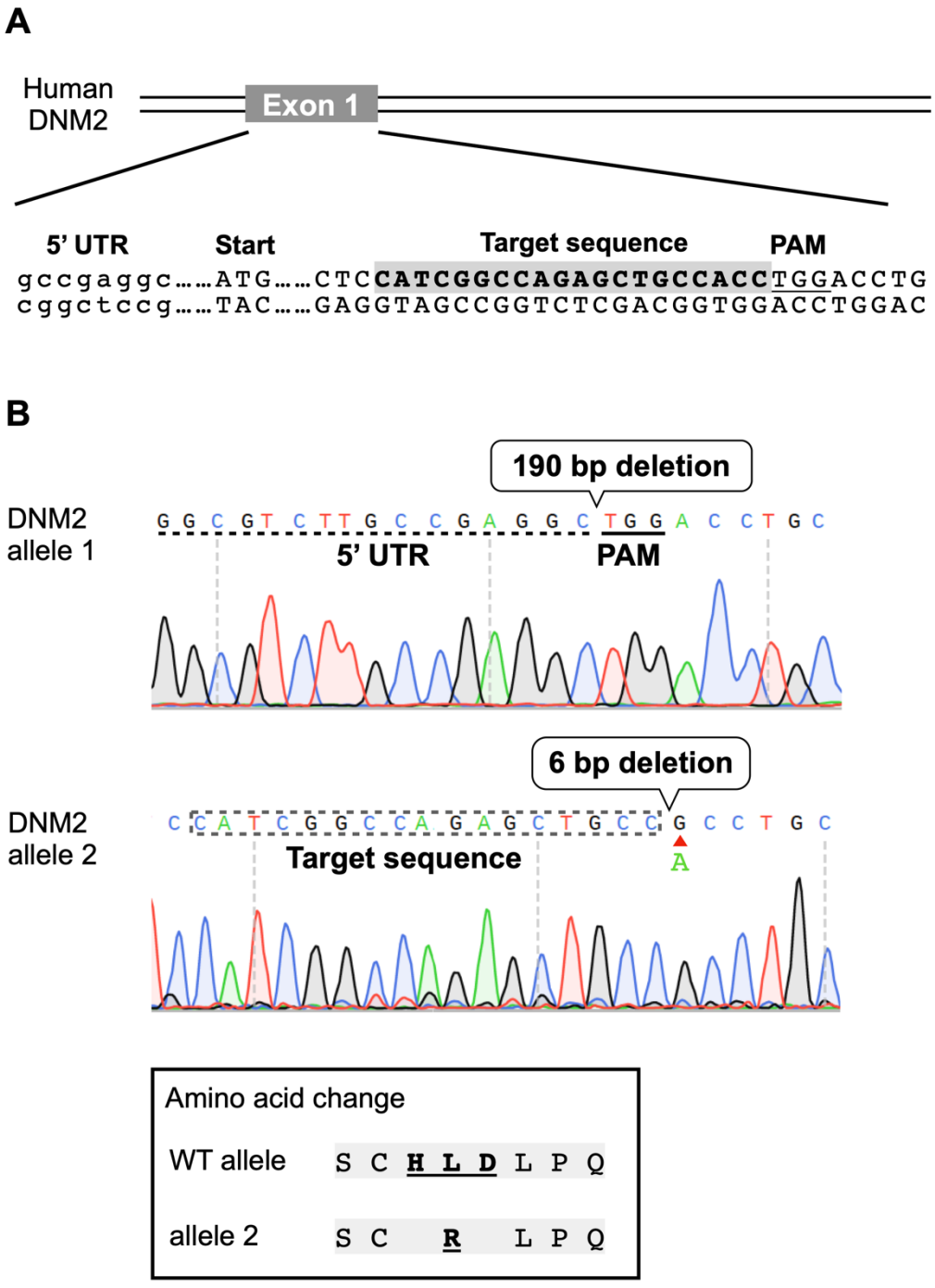

Figure 1. Generation of a heterozygous *DNM2* mutant (*DNM2*$^{HLD>R/-}$) cell line by CRISPR/Cas9 system. **(A)** Schematic diagrams of human *DNM2* gene. Target sequence in exon 1 is highlighted and followed by a PAM sequence. **(B)** Sequencing chromatogram of *DNM2*$^{HLD>R/-}$ cell line. On one of the *DNM2* alleles, 190 base pairs containing the start codon and about a half of 5'UTR were deleted. Another allele has a 6-base-pair deletion and a single base-pair substitution. The box shows the protein sequence near the deletion/substitution sites on allele 2.

Figure 2

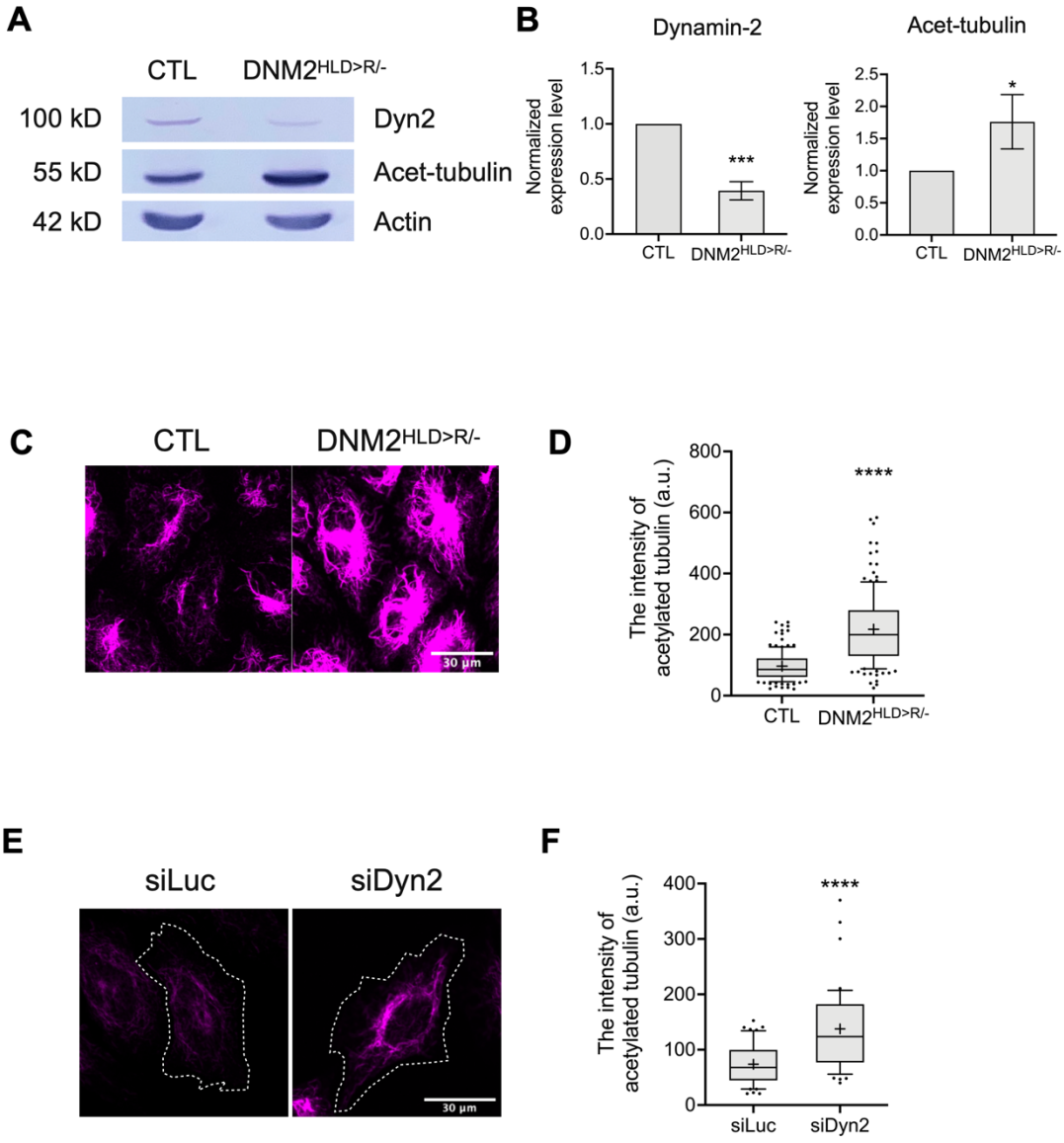
A
CTL
DNM2HLD>R/-
100 kD
55 kD
42 kD
Dyn2
Acet-tubulin
Actin
B
Dynamin-2
Acet-tubulin
Normalized expression level
1.5
1.0
0.5
0.0
***
CTL
DNM2HLD>R/-
2.5
2.0
1.5
1.0
0.5
0.0
*
C
CTL
DNM2HLD>R/-
30 µm
D
The intensity of acetylated tubulin (a.u.)
800
600
400
200
0
****
CTL
DNM2HLD>R/-
E
siLuc
siDyn2
30 µm
F
The intensity of acetylated tubulin (a.u.)
400
300
200
100
0
****
siLuc
siDyn2

Figure 2. *DNM2* heterozygous mutation leads to increased microtubule stabilization. **(A)** Immunoblotting of cell lysates from control (CTL) or heterozygous *DNM2* mutant (*DNM2*$^{HLD>R/-}$) HeLa cells with anti-dynamin-2 (Dyn2), anti-acetylated tubulin (Acet-tubulin), and anti-actin antibodies. **(B)** The protein levels of dynamin-2 and acetylated tubulin in *DNM2*$^{HLD>R/-}$ cells were quantified and normalized to those of CTL cells. Actin was used as the loading control. Each bar represents the mean ± SD from three independent experiments (n = 3). Unpaired Student's t-test was performed to compare the expression of dynamin-2 and acetylated tubulin in *DNM2*$^{HLD>R/-}$ cells with that in CTL cells (*$p < 0.05$, ***$p < 0.001$). **(C)** CTL or *DNM2*$^{HLD>R/-}$ cells were immunostained with anti-acetylated tubulin antibody (magenta). Scale bar = 30 μm. **(D)** The intensity of acetylated tubulin was quantified and shown in a boxplot. The top, middle and bottom lines of the box represent 90%, 50% and 10% of data, respectively. The boxplot whiskers are SD. The mean is shown as a symbol (+). Unpaired Student's t-test was performed to compare the levels of acetylated tubulin in *DNM2*$^{HLD>R/-}$ cells (n = 143) with that in CTL cells (n = 146) (****$p < 0.0001$). **(E)** siRNA against dynamin-2 (siDyn2, sequence: GGGCUUCAUGUCCAACAAG) or Luciferase (siLuc, sequence: CGUACGCGGAAUACUUCGA) was transfected into HeLa cells by Nucleofector™ Kit R (#VVCA-1001, Lonza, Basel, Switzerland). Transfected HeLa cells were immunostained with anti-acetylated tubulin antibody (magenta). The outline of the cells is framed by the dashed line. Scale bar = 30 μm. **(F)** The intensity of acetylated tubulin was quantified and shown in a boxplot. Unpaired Student's t test was performed to compare the intensity of acetylated tubulin in the cells transfected with siDyn2 (n = 49) with that in the cells transfected with siLuc (n = 56) (****$p< 0.0001$).

Figure 3

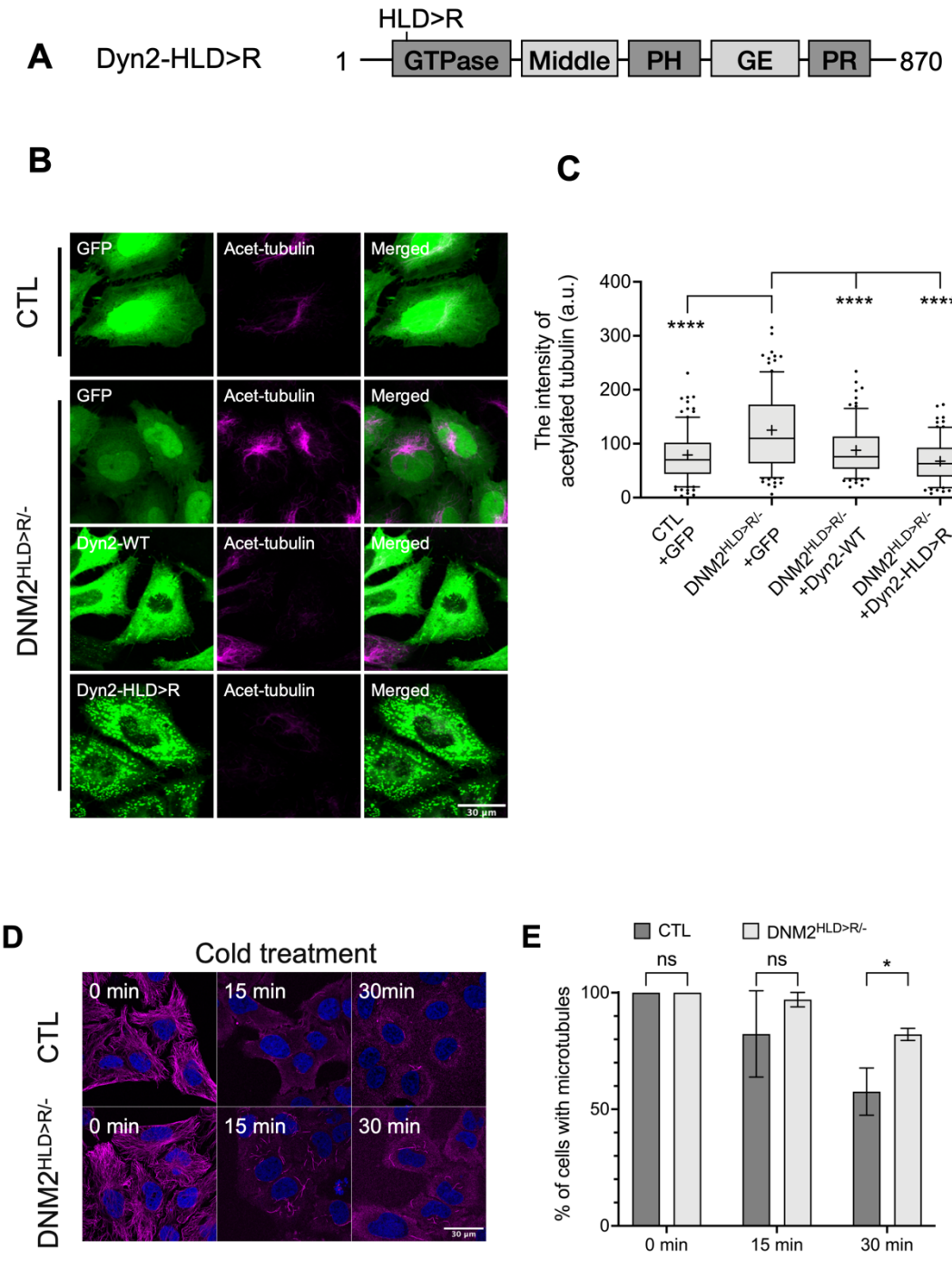
A
Dyn2-HLD>R
HLD>R
1
GTPase
Middle
PH
GE
PR
870
B
CTL
DNM2HLD>R/-
GFP
Acet-tubulin
Merged
Dyn2-WT
Dyn2-HLD>R
30 µm
C
The intensity of acetylated tubulin (a.u.)
400
300
200
100
0
****
****
****
CTL +GFP
DNM2HLD>R/- +GFP
DNM2HLD>R/- +Dyn2-WT
DNM2HLD>R/- +Dyn2-HLD>R
D
Cold treatment
CTL
DNM2HLD>R/-
0 min
15 min
30min
30 min
30 µm
E
CTL
DNM2HLD>R/-
% of cells with microtubules
100
50
0
ns
ns
*
0 min
15 min
30 min

Figure 3. Effect of GFP-dynamin-2-WT and -HLD>R expression on microtubule stabilization in *DNM2*$^{HLD>R/-}$ HeLa cells. **(A)** Schematic diagram of dynamin-2-HLD>R mutant. pEGFP-C1-*DNM2*-HLD>R was generated by PCR-based mutagenesis using pEGFP-C1-DNM2-WT as a template. **(B)** CTL or *DNM2*$^{HLD>R/-}$ HeLa cells expressing GFP, GFP-dynamin-2-WT, or -HLD>R (green) were immunostained with anti-acetylated tubulin antibody (magenta). Scale bar = 30 μm. **(C)** The intensity of acetylated tubulin was quantified and shown in a boxplot. The top, middle and bottom lines of the box represent 90%, 50% and 10% of data, respectively. The boxplot whiskers are SD. The mean is shown as a symbol (+). One-way ANOVA (Dunnett's multiple comparisons test) was performed to compare the intensity of acetylated tubulin in CTL cells expressing GFP (n = 104) or *DNM2*$^{HLD>R/-}$ HeLa cells expressing GFP-dynamin-2-WT/-HLD>R (n ≥ 90) with that in *DNM2*$^{HLD>R/-}$ HeLa cells expressing GFP (n = 108) (****p< 0.0001). **(D)** CTL or *DNM2*$^{HLD>R/–}$ cells were treated on ice for 0, 15, or 30 min and then immunostained with anti-α-tubulin antibody (magenta). Nuclei were stained with DAPI (blue). Scale bar = 30 μm. **(E)** The number of cells in (D) that have more than one filamentous structure was divided by total cell number (n ≥ 34). Each bar represents the mean ± SD from three independent experiments (n = 3). Statistical significance was performed using two-way ANOVA (bonferroni's multiple comparison test) (*p < 0.05).

Figure 4

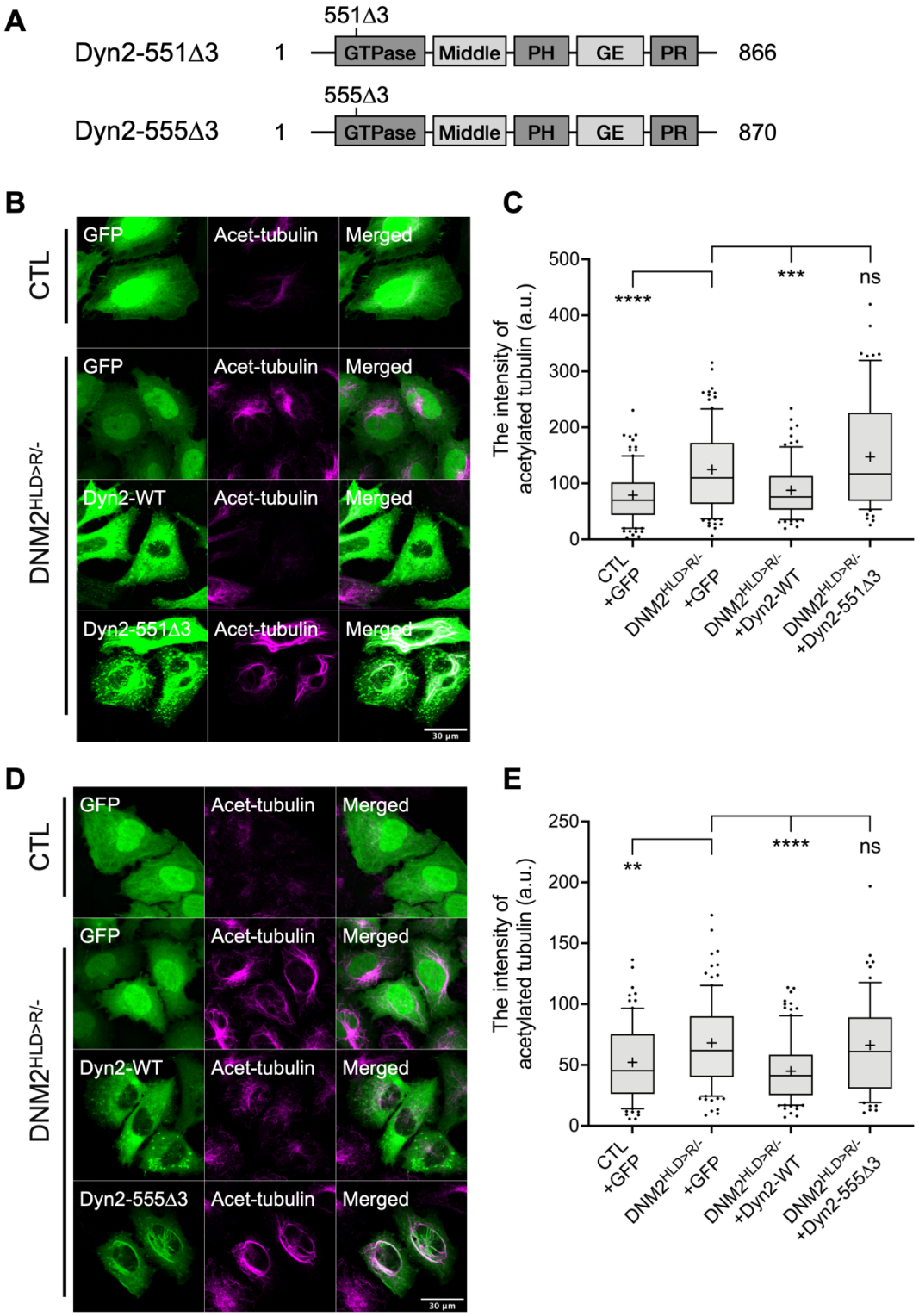
A
551Δ3
Dyn2-551Δ3
1
GTPase
Middle
PH
GE
PR
866
555Δ3
Dyn2-555Δ3
1
GTPase
Middle
PH
GE
PR
870
B
CTL
DNM2HLD>R/-
GFP
Acet-tubulin
Merged
GFP
Acet-tubulin
Merged
Dyn2-WT
Acet-tubulin
Merged
Dyn2-551Δ3
Acet-tubulin
Merged
30 μm
C
The intensity of acetylated tubulin (a.u.)
500
400
300
200
100
0
****
***
ns
CTL +GFP
DNM2HLD>R/- +GFP
DNM2HLD>R/- +Dyn2-WT
DNM2HLD>R/- +Dyn2-551Δ3
D
CTL
DNM2HLD>R/-
GFP
Acet-tubulin
Merged
GFP
Acet-tubulin
Merged
Dyn2-WT
Acet-tubulin
Merged
Dyn2-555Δ3
Acet-tubulin
Merged
30 μm
E
The intensity of acetylated tubulin (a.u.)
250
200
150
100
50
0
**
****
ns
CTL +GFP
DNM2HLD>R/- +GFP
DNM2HLD>R/- +Dyn2-WT
DNM2HLD>R/- +Dyn2-555Δ3

Figure 4. Effect of dynamin-2-551Δ3 and -555Δ3 mutant expressions on microtubule stabilization in *DNM2*$^{HLD>R/-}$ HeLa cells. **(A)** Schematic diagram of dynamin-2-551Δ3 and -555Δ3 mutants. **(B and D)** CTL or *DNM2*$^{HLD>R/-}$ HeLa cells expressing GFP, GFP-dynamin-2-WT, -551Δ3 (B, green), or -555Δ3 (D, green) were immunostained with anti-acetylated tubulin antibody (magenta). Scale bars = 30 μm. **(C and E)** The intensity of acetylated tubulin was quantified and shown in a boxplot. The top, middle and bottom lines of the box represent 90%, 50% and 10% of data, respectively. The boxplot whiskers are SD. The mean is shown as a symbol (+). One-way ANOVA (Dunnett's multiple comparisons test) was performed to compare the intensity of acetylated tubulin in CTL cells expressing GFP ($n \geq 100$) or *DNM2*$^{HLD>R/-}$ HeLa cells expressing GFP-dynamin-2-WT/mutants ($n \geq 90$) with *DNM2*$^{HLD>R/-}$ HeLa cells expressing GFP ($n \geq 73$) (**$p < 0.01$, ***$p < 0.001$, ****$p < 0.0001$).

Figure 5

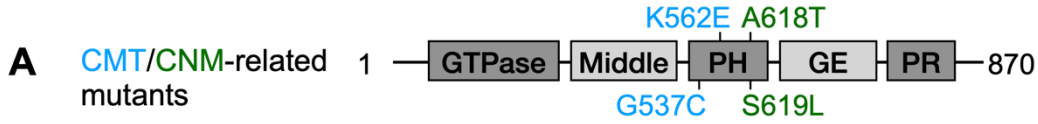
A
CMT/CNM-related mutants
1
GTPase
Middle
PH
GE
PR
870
K562E
A618T
G537C
S619L

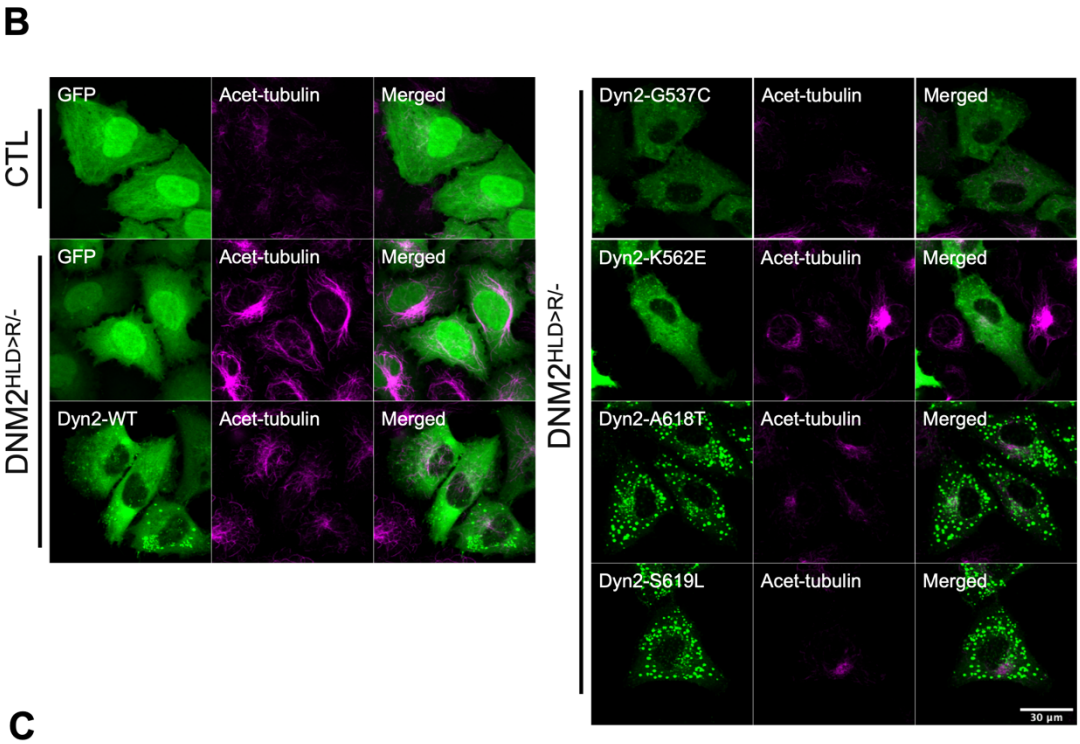
B
CTL
DNM2HLD>R/-
GFP
Acet-tubulin
Merged
Dyn2-WT
Dyn2-G537C
Dyn2-K562E
Dyn2-A618T
Dyn2-S619L
30 μm

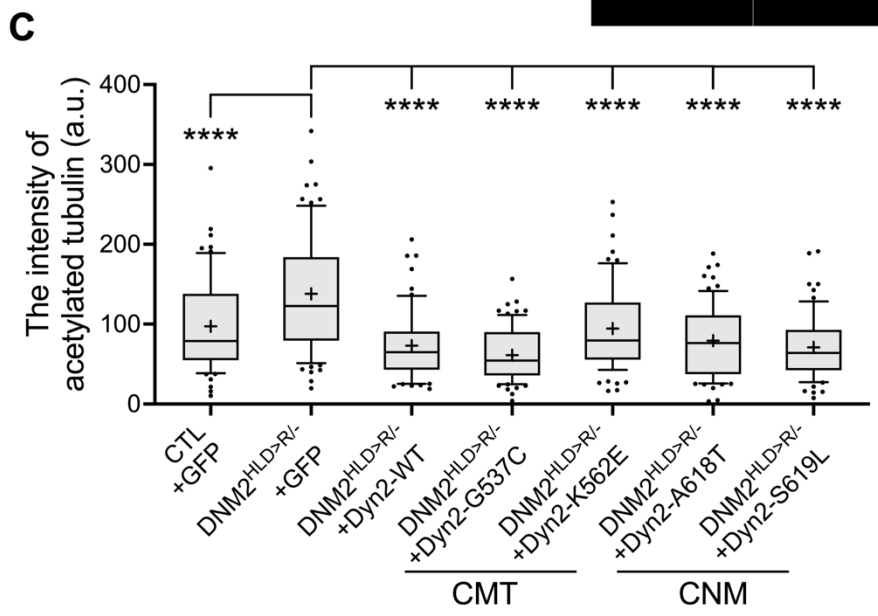
C
The intensity of acetylated tubulin (a.u.)
400
300
200
100
0
****
CTL +GFP
DNM2HLD>R/- +GFP
DNM2HLD>R/- +Dyn2-WT
DNM2HLD>R/- +Dyn2-G537C
DNM2HLD>R/- +Dyn2-K562E
DNM2HLD>R/- +Dyn2-A618T
DNM2HLD>R/- +Dyn2-S619L
CMT
CNM

Figure 5. Effect of GFP-dynamin-2-G537C, -K562E, -A618T and -S619L mutant expressions on microtubule stabilization in *DNM2*$^{HLD>R/-}$ HeLa cells. **(A)** Schematic diagram of dynamin-2-G537C, -K562E, -A618T and -S619L mutants. pEGFP-C1-*DNM2*-mutant was generated by PCR-based mutagenesis using pEGFP-C1-*DNM2*-WT as a template. Charcot-Marie-Tooth disease (CMT) or Centronuclear myopathy (CNM)-related mutants are shown in blue or green, respectively. **(B)** CTL or *DNM2*$^{HLD>R/-}$ HeLa cells expressing GFP, GFP-dynamin-2-WT, or mutants (green) were immunostained with anti-acetylated tubulin antibody (magenta). Scale bar = 30 μm. **(C)** The intensity of acetylated tubulin was quantified and shown in a boxplot. The top, middle and bottom lines of the box represent 90%, 50% and 10% of data, respectively. The boxplot whiskers are SD. The mean is shown as a symbol (+). One-way ANOVA (Dunnett's multiple comparisons test) was performed to compare the intensity of acetylated tubulin in CTL cells expressing GFP (n = 65) or *DNM2*$^{HLD>R/-}$ HeLa cells expressing GFP-dynamin-2-WT/mutants (n ≥ 40) with *DNM2*$^{HLD>R/-}$ HeLa cells expressing GFP (n = 73) (****$p < 0.0001$).

Figure 6

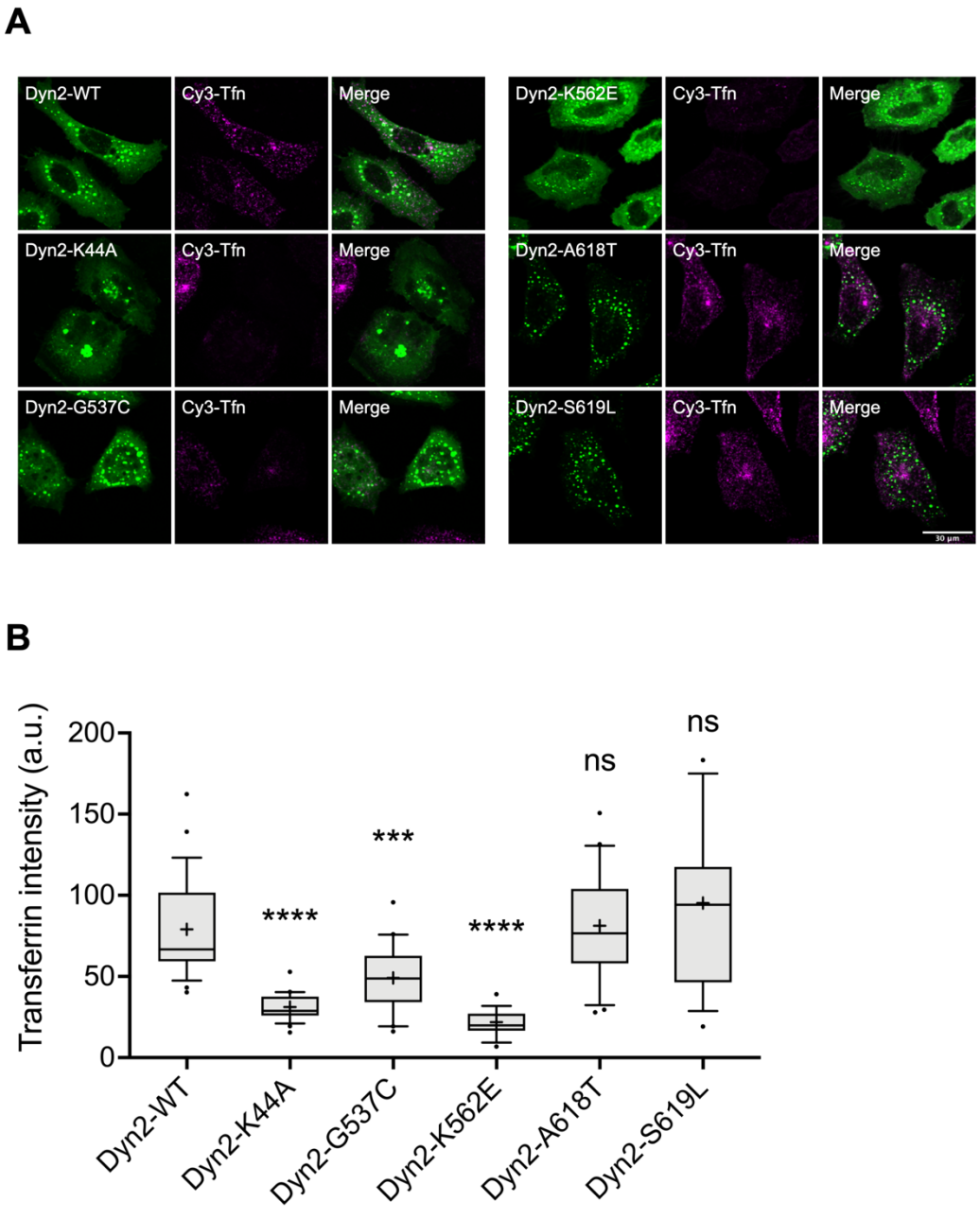
A
Dyn2-WT
Cy3-Tfn
Merge
Dyn2-K562E
Cy3-Tfn
Merge
Dyn2-K44A
Cy3-Tfn
Merge
Dyn2-A618T
Cy3-Tfn
Merge
Dyn2-G537C
Cy3-Tfn
Merge
Dyn2-S619L
Cy3-Tfn
Merge
30 µm
B
Transferrin intensity (a.u.)
200
150
100
50
0
****
***
****
ns
ns
Dyn2-WT
Dyn2-K44A
Dyn2-G537C
Dyn2-K562E
Dyn2-A618T
Dyn2-S619L

Figure 6. Effect of GFP-dynamin-2-K44A, -G537C, -K562E, -A618T, and -S619L expressions on Cy3-transferrin uptake in HeLa cells. **(A)** HeLa cells expressing GFP-dynamin-2-WT or indicated mutants (green) were incubated with 25 μg/mL of Cy3-transferrin (Cy3-Tfn, magenta) for 30 min before fixation. The images were obtained using Olympus FV1000 with UPLSAPO 40×/0.90 objective. Scale bar = 30 μm. **(B)** The intensity of Cy3-transferrin was quantified by Fiji software and shown in a boxplot. The top, middle and bottom lines of the box represent 90%, 50% and 10% of data, respectively. The boxplot whiskers are SD. The mean is shown as a symbol (+). One-way ANOVA (Dunnett's multiple comparisons test) was performed to compare the intensity of Cy3-transferrin in the cells expressing GFP-dynamin-2 mutants ($n \geq 15$) with that in the cells expressing GFP-dynamin-2-WT ($n = 28$) (***$p < 0.001$, ****$p < 0.0001$).

Figure 7

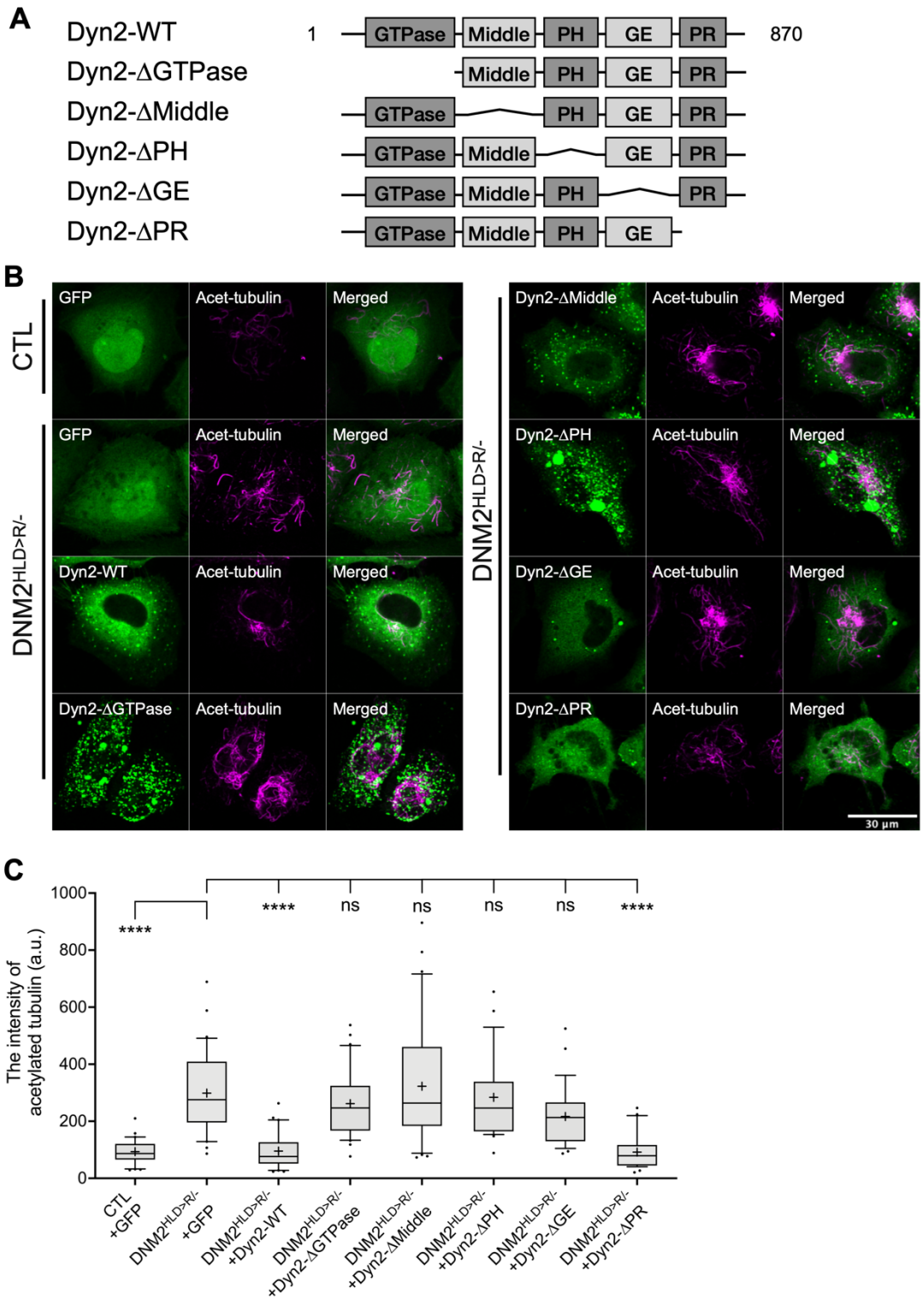
A
Dyn2-WT
Dyn2-ΔGTPase
Dyn2-ΔMiddle
Dyn2-ΔPH
Dyn2-ΔGE
Dyn2-ΔPR
1
870
GTPase
Middle
PH
GE
PR
B
CTL
DNM2HLD>R/-
GFP
Acet-tubulin
Merged
Dyn2-WT
Dyn2-ΔGTPase
Dyn2-ΔMiddle
Dyn2-ΔPH
Dyn2-ΔGE
Dyn2-ΔPR
30 μm
C
The intensity of acetylated tubulin (a.u.)
1000
800
600
400
200
0
****
ns
CTL +GFP
DNM2HLD>R/- +GFP
DNM2HLD>R/- +Dyn2-WT
DNM2HLD>R/- +Dyn2-ΔGTPase
DNM2HLD>R/- +Dyn2-ΔMiddle
DNM2HLD>R/- +Dyn2-ΔPH
DNM2HLD>R/- +Dyn2-ΔGE
DNM2HLD>R/- +Dyn2-ΔPR

Figure 7. Effect of GFP-dynamin-2-ΔGTPase, -ΔMiddle, -ΔPH, -ΔGE, and -ΔPR mutant expressions on microtubule stabilization in *DNM2*$^{HLD>R/-}$ HeLa cells. **(A)** Schematic diagram of dynamin-2-WT and dynamin-2 domain-deleted mutants: ΔGTPase, ΔMiddle, ΔPH, ΔGE, and ΔPR. **(B)** CTL or *DNM2*$^{HLD>R/-}$ HeLa cells expressing GFP, GFP-dynamin-2-WT, or mutants (green) were immunostained with anti-acetylated tubulin antibody (magenta). Scale bar = 30 μm. **(C)** The intensity of acetylated tubulin was quantified and shown in a boxplot. The top, middle and bottom lines of the box represent 90%, 50% and 10% of data, respectively. The boxplot whiskers are SD. The mean is shown as a symbol (+). One-way ANOVA (Dunnett's multiple comparisons test) was performed to compare the intensity of acetylated tubulin in CTL cells expressing GFP (n = 30) or *DNM2*$^{HLD>R/-}$ HeLa cells expressing GFP-dynamin-2-WT/mutants ($n \geq 20$) with *DNM2*$^{HLD>R/-}$ HeLa cells expressing GFP (n = 30) (****$p < 0.0001$).

Figure 8

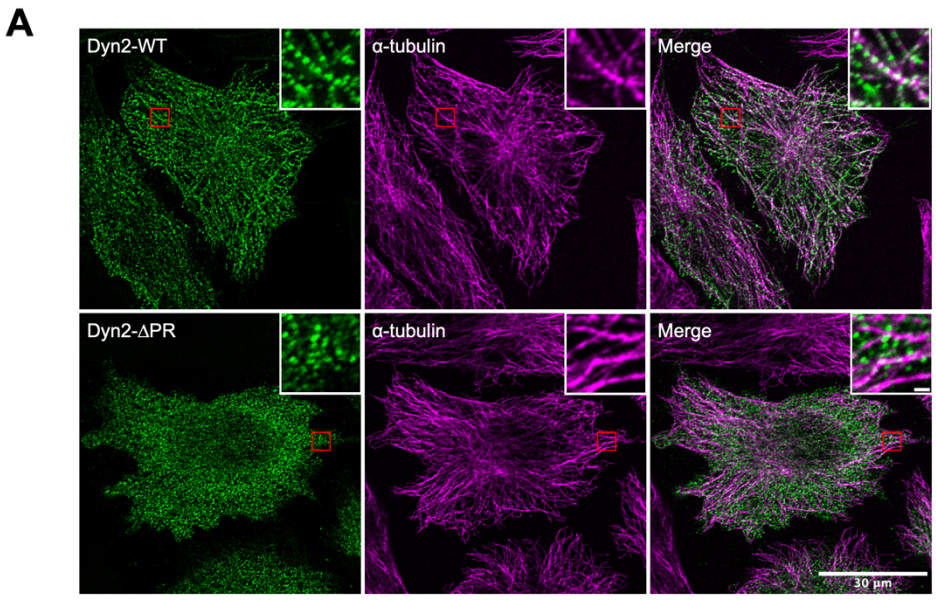
A
Dyn2-WT
α-tubulin
Merge
Dyn2-ΔPR
α-tubulin
Merge
30 μm
B
Pearson's Correlation Coeffecient
0.4
0.3
0.2
0.1
0.0
*
Dyn2-WT
Dyn2-ΔPR

Figure 8. Co-localization analysis of GFP-dynamin-2-WT and -ΔPR with microtubules. **(A)** HeLa cells expressing GFP-dynamin-2-WT, or -ΔPR mutant (green) were pre-permeabilized in warmed BRB80 (80 mM Pipes/KOH, pH 6.8, 1 mM $MgCl_2$, 1 mM EGTA, 4% polyethylene glycol 8000) with 0.3% Triton X-100 for 10 min before fixation. Then, the cells were immunostained with anti-α-tubulin antibody (magenta). The images were obtained using ZEISS LSM 900 with Plan-Apochromat 63×/1.40 Oil M27 Objective. The inset image in each channel displays a magnified view of the boxed region. Scale bar = 30 μm. Scale bar of inset image = 1 μm. **(B)** The co-localization of GFP-dynamin-2-WT or -ΔPR mutant with microtubules was quantified by measuring the Pearson's correlation coefficient using Volocity software (v. 6.5.1; PerkinElmer, MA, USA). Each bar represents the mean (n = 10) ± SD. Statistical significance was performed using unpaired t-tests (*$p < 0.05$).

Figure 9

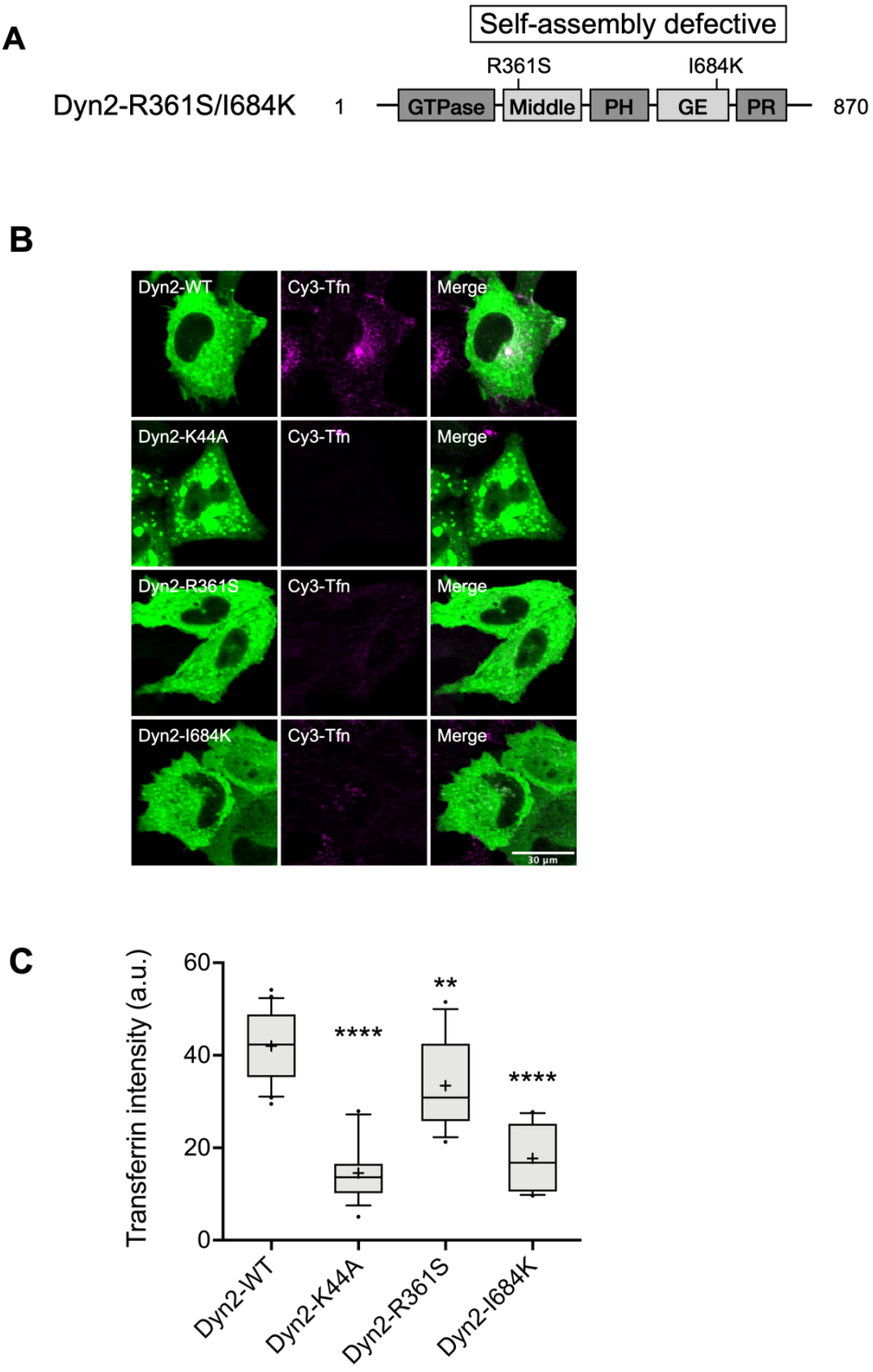
A
Self-assembly defective
R361S
I684K
Dyn2-R361S/I684K
1
GTPase
Middle
PH
GE
PR
870
B
Dyn2-WT
Cy3-Tfn
Merge
Dyn2-K44A
Cy3-Tfn
Merge
Dyn2-R361S
Cy3-Tfn
Merge
Dyn2-I684K
Cy3-Tfn
Merge
30 µm
C
Transferrin intensity (a.u.)
60
40
20
0
****
**
****
Dyn2-WT
Dyn2-K44A
Dyn2-R361S
Dyn2-I684K

Figure 9. Effect of GFP-dynamin-2-K44A, -R361S and I684K expressions on Cy3-transferrin uptake in HeLa cells. **(A)** Schematic diagram of dynamin-2 mutants, R361S and I684K. **(B)** HeLa cells expressing GFP-dynamin-2-WT or mutants (green) were incubated with 25 μg/mL of Cy3-transferrin (Cy3-Tfn, magenta) for 30 min before fixation. The images were obtained using Olympus FV1000 with UPLSAPO 40×/0.90 objective. Scale bar = 30 μm. **(C)** The intensity of Cy3-transferrin was quantified by Fiji software and shown in a boxplot. The top, middle and bottom lines of the box represent 90%, 50% and 10% of data, respectively. The boxplot whiskers are SD. The mean is shown as a symbol (+). One-way ANOVA (Dunnett's multiple comparisons test) was performed to compare the intensity of Cy3-transferrin in the cells expressing GFP-dynamin-2 mutants ($n \geq 15$) with that in the cells expressing GFP-dynamin-2-WT ($n = 28$) (**$p < 0.01$, ****$p < 0.0001$).

Figure 10

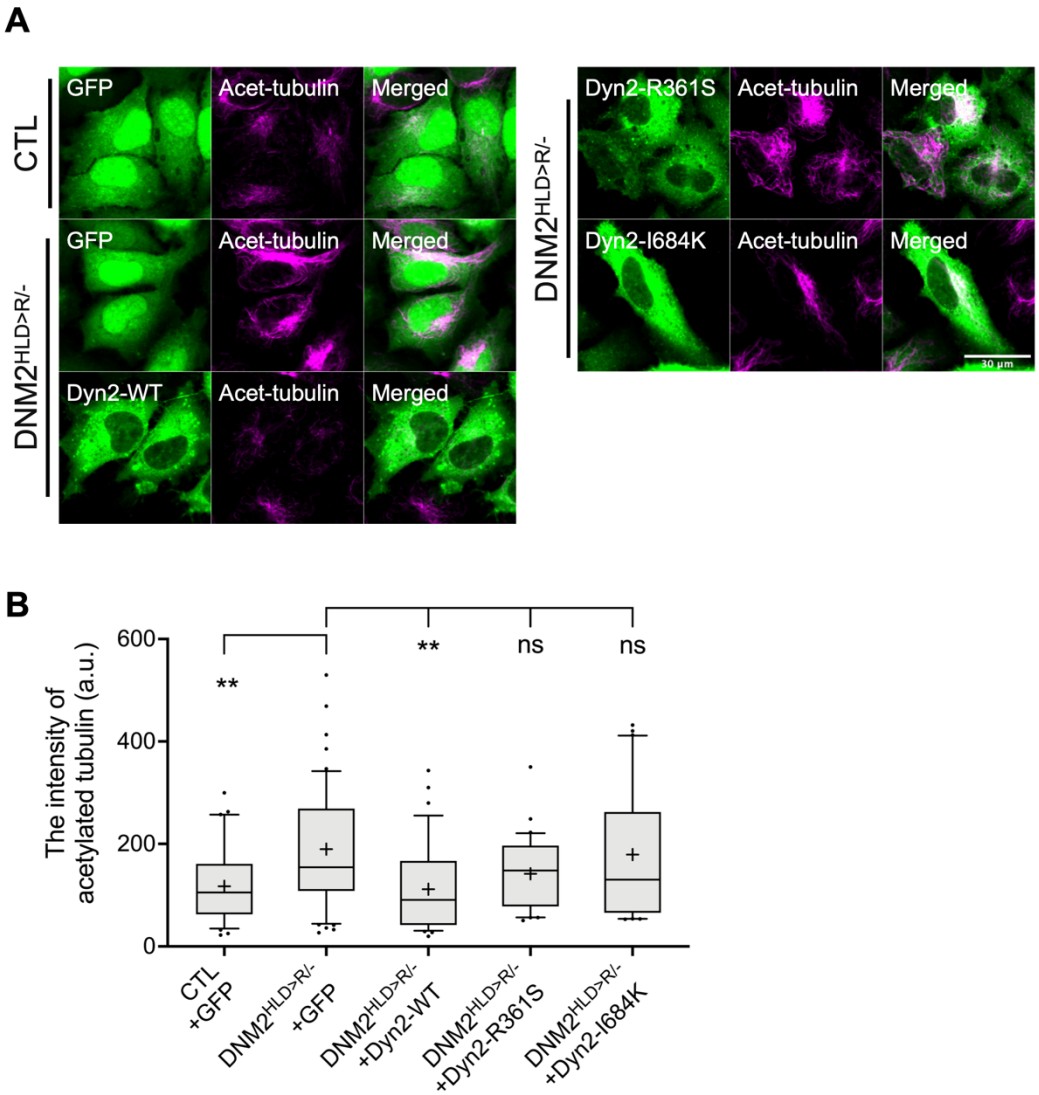
A
CTL
GFP
Acet-tubulin
Merged
DNM2HLD>R/-
GFP
Acet-tubulin
Merged
Dyn2-WT
Acet-tubulin
Merged
DNM2HLD>R/-
Dyn2-R361S
Acet-tubulin
Merged
Dyn2-I684K
Acet-tubulin
Merged
30 μm
B
The intensity of acetylated tubulin (a.u.)
600
400
200
0
**
**
ns
ns
CTL +GFP
DNM2HLD>R/- +GFP
DNM2HLD>R/- +Dyn2-WT
DNM2HLD>R/- +Dyn2-R361S
DNM2HLD>R/- +Dyn2-I684K

Figure 10. Effect of GFP-dynamin-2-R361S and -I684K mutant expressions on microtubule stabilization in *DNM2*$^{HLD>R/-}$ HeLa cells. **(A)** CTL or *DNM2*$^{HLD>R/-}$ HeLa cells expressing GFP, GFP-dynamin-2-WT, or mutants (green) were immunostained with anti-acetylated tubulin antibody (magenta). Scale bar = 30 μm. **(B)** The intensity of acetylated tubulin was quantified and shown in a boxplot. The top, middle and bottom lines of the box represent 90%, 50% and 10% of data, respectively. The boxplot whiskers are SD. The mean is shown as a symbol (+). One-way ANOVA (Dunnett's multiple comparisons test) was performed to compare the intensity of acetylated tubulin in CTL cells expressing GFP (n = 24) or *DNM2*$^{HLD>R/-}$ HeLa cells expressing GFP-dynamin-2-WT/mutants ($n \geq 20$) with *DNM2*$^{HLD>R/-}$ HeLa cells expressing GFP (n = 53) (**$p < 0.01$).

Figure 11

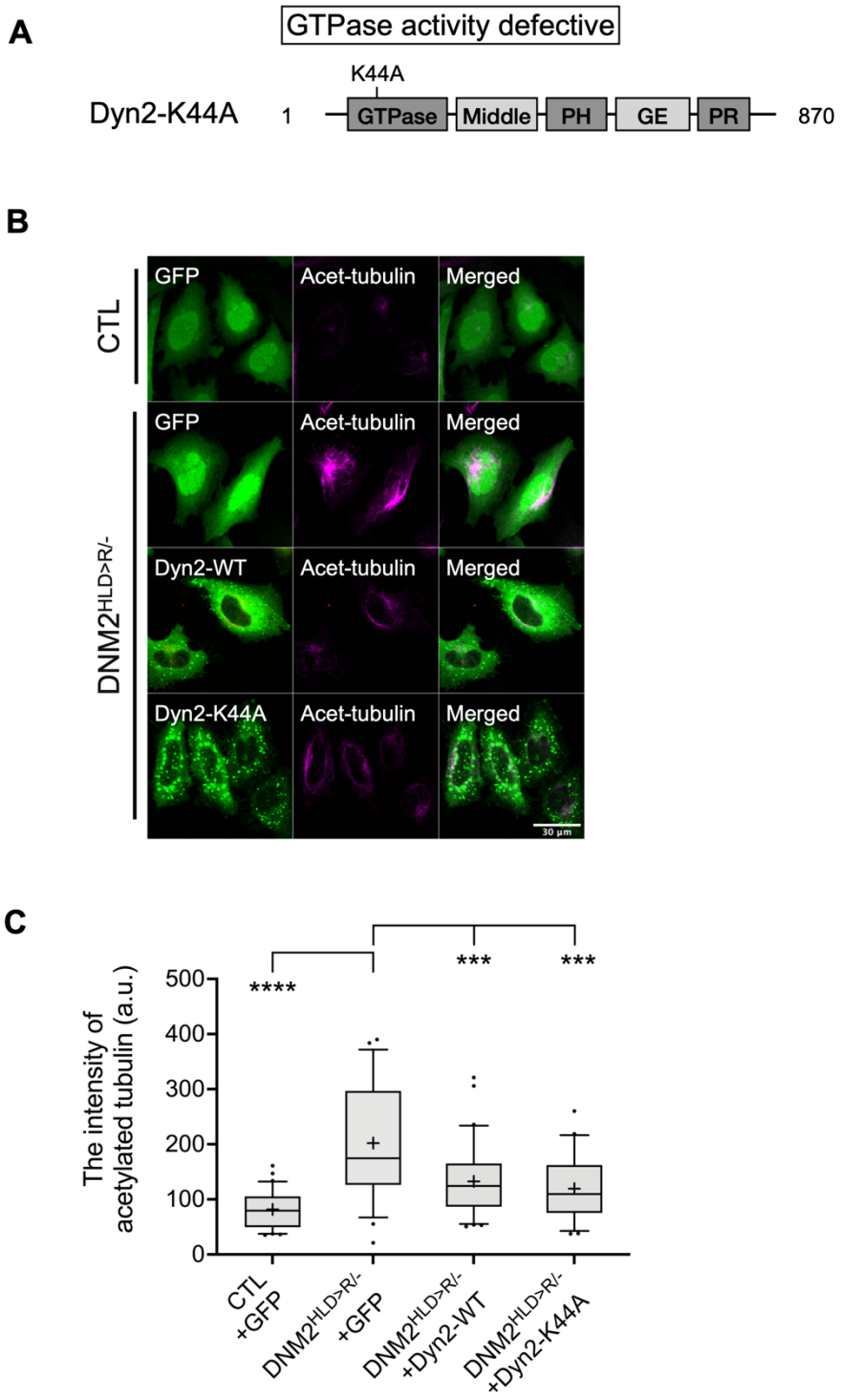
A
GTPase activity defective
K44A
Dyn2-K44A
1
GTPase
Middle
PH
GE
PR
870
B
CTL
DNM2HLD>R/-
GFP
Acet-tubulin
Merged
Dyn2-WT
Dyn2-K44A
30 µm
C
The intensity of acetylated tubulin (a.u.)
500
400
300
200
100
0
****
***
***
CTL +GFP
DNM2HLD>R/- +GFP
DNM2HLD>R/- +Dyn2-WT
DNM2HLD>R/- +Dyn2-K44A

Figure 11. Effect of dynamin-2-K44A mutant expression on microtubule stabilization in *DNM2*$^{HLD>R/-}$ HeLa cells. **(A)** Schematic diagram of dynamin-2-K44A mutant. **(B)** CTL or *DNM2*$^{HLD>R/-}$ HeLa cells expressing GFP, GFP-dynamin-2-WT, or -K44A (green) were immunostained with anti-acetylated tubulin antibody (magenta). Scale bar = 30 μm. **(C)** The intensity of acetylated tubulin was quantified and shown in a boxplot. The top, middle and bottom lines of the box represent 90%, 50% and 10% of data, respectively. The boxplot whiskers are SD. The mean is shown as a symbol (+). One-way ANOVA (Dunnett's multiple comparisons test) was performed to compare the intensity of acetylated tubulin in CTL cells expressing GFP (n = 35) or *DNM2*$^{HLD>R/-}$ HeLa cells expressing GFP-dynamin-2-WT/-K44A ($n \geq 20$) with *DNM2*$^{HLD>R/-}$ HeLa cells expressing GFP (n = 26) (***$p < 0.001$, ****$p < 0.0001$).

Figure 12

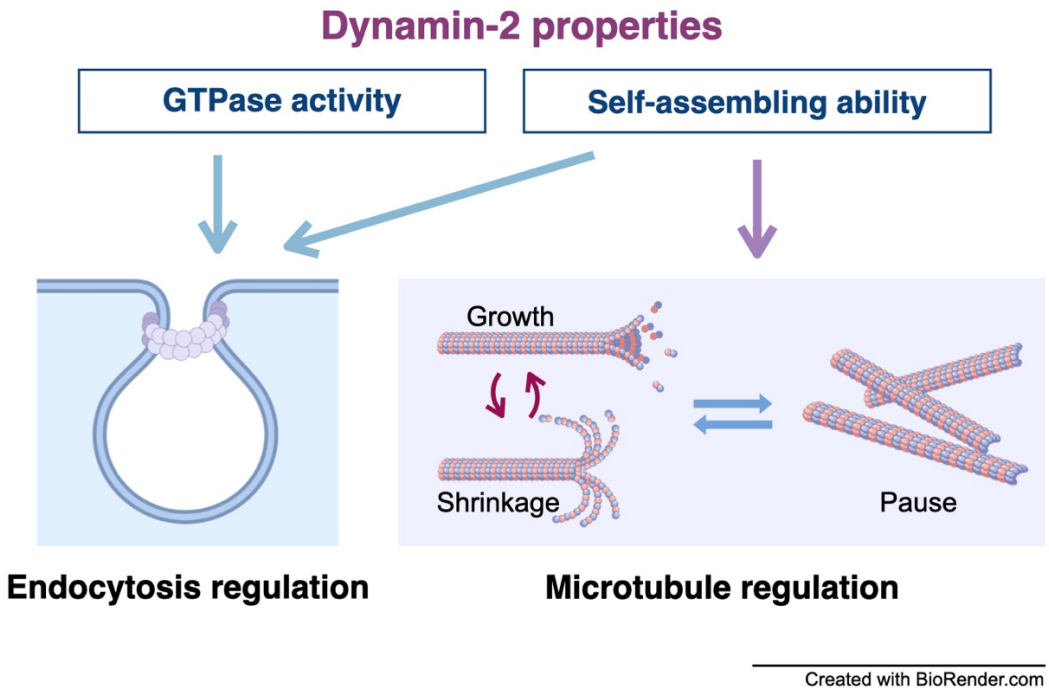

Figure 12. This study's graphical summary concludes distinct dynamin-2-dependent regulatory mechanisms between microtubule stability and endocytosis.

Figure 13

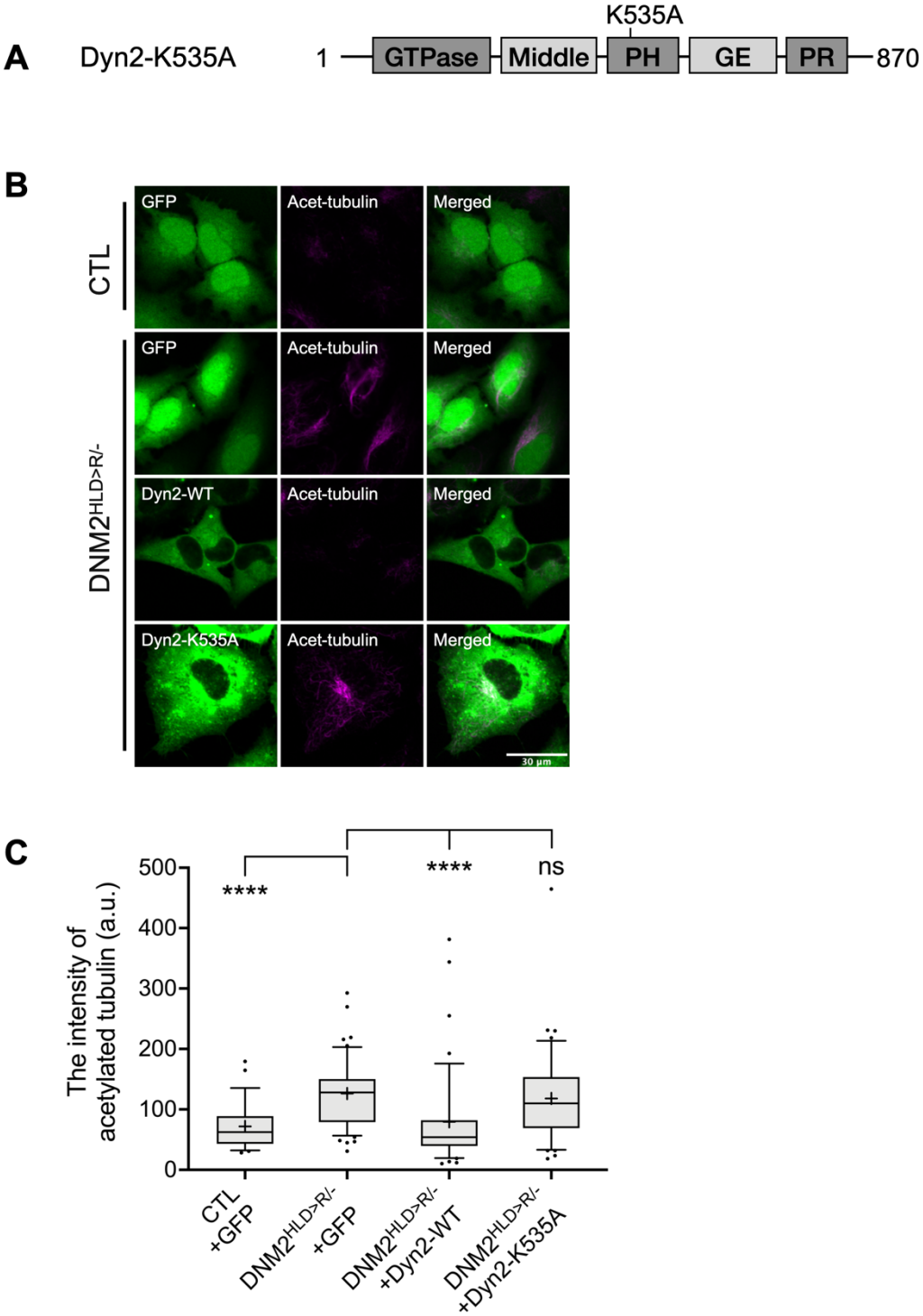
A
Dyn2-K535A
1
GTPase
Middle
K535A
PH
GE
PR
870
B
CTL
DNM2HLD>R/-
GFP
Acet-tubulin
Merged
Dyn2-WT
Dyn2-K535A
30 μm
C
The intensity of acetylated tubulin (a.u.)
500
400
300
200
100
0
****
****
ns
CTL +GFP
DNM2HLD>R/- +GFP
DNM2HLD>R/- +Dyn2-WT
DNM2HLD>R/- +Dyn2-K535A

Figure 13. Effect of GFP-dynamin-2-K535A expression on microtubule stabilization in *DNM2*$^{HLD>R/-}$ HeLa cells. **(A)** Schematic diagram of dynamin-2-K535A mutant. **(B)** CTL or *DNM2*$^{HLD>R/-}$ HeLa cells expressing GFP, GFP-dynamin-2-WT, or -K535A (green) were immunostained with anti-acetylated tubulin antibody (magenta). Scale bar = 30 μm. **(C)** The intensity of acetylated tubulin was quantified and shown in a boxplot. The top, middle and bottom lines of the box represent 90%, 50% and 10% of data, respectively. The boxplot whiskers are SD. The mean is shown as a symbol (+). One-way ANOVA (Dunnett's multiple comparisons test) was performed to compare the intensity of acetylated tubulin in CTL cells expressing GFP (n = 24) or *DNM2*$^{HLD>R/-}$ HeLa cells expressing GFP-dynamin-2-WT/-K535A (n ≥ 40) with that in *DNM2*$^{HLD>R/-}$ HeLa cells expressing GFP (n = 53) (****$p < 0.0001$).

Table 1

Table 1. Characters of dynamin-2 mutants and their effects on abnormal stabilized microtubule in *DNM2*$^{HLD>R/-}$ HeLa cells.

Dynamin-2 mutant	Character	Rescue abnormal stabilized microtubule
ΔGTPase, ΔMiddle, ΔGE, ΔPH	Domain deletion	−
ΔPR	Domain deletion	+
K44A	GTPase activity defect[1]	+
R361S	Self-assembly defect[2]	−
I684K	Self-assembly defect[3]	−
K535A	Lipid-binding defect[4]	−
551Δ3 (555Δ3)	CMT disease	−
G537C, K562E	CMT disease	+
A618T, S619L	CNM	+

CMT: Charcot-Marie-Tooth; CNM: centronuclear myopathy.

Reference:

1. Damke, Baba, Warnock, & Schmid, 1994
2. Ramachandran et al., 2007
3. Song, Yarar, & Schmid, 2004
4. Vallis, Wigge, Marks, Evans, & McMahon, 1999